NASA TECHNICAL NOTE

NASA TN D-4344

NASA TN D-4344
c.1

LOAN COPY: RET
AF[illegible] (WLI
KIRTLAND AFB,

TECH LIBRARY KAFB, NM
0131485

CALCULATION OF THE DYNAMIC LONGITUDINAL STABILITY OF A TILT-WING V/STOL AIRCRAFT AND CORRELATION WITH MODEL FLIGHT TESTS

by Joseph R. Chambers and Sue B. Grafton

Langley Research Center
Langley Station, Hampton, Va.

NATIONAL AERONAUTICS AND SPACE ADMINISTRATION • WASHINGTON, D. C. • FEBRUARY 1968

TECH LIBRARY KAFB, NM
0131485

CALCULATION OF THE DYNAMIC LONGITUDINAL STABILITY OF A TILT-WING V/STOL AIRCRAFT AND CORRELATION WITH MODEL FLIGHT TESTS

By Joseph R. Chambers and Sue B. Grafton

Langley Research Center
Langley Station, Hampton, Va.

NATIONAL AERONAUTICS AND SPACE ADMINISTRATION

For sale by the Clearinghouse for Federal Scientific and Technical Information
Springfield, Virginia 22151 – CFSTI price $3.00

CALCULATION OF THE DYNAMIC LONGITUDINAL STABILITY OF A TILT-WING V/STOL AIRCRAFT AND CORRELATION WITH MODEL FLIGHT TESTS

By Joseph R. Chambers and Sue B. Grafton
Langley Research Center

SUMMARY

An analytical study has been conducted to determine the important factors influencing the dynamic longitudinal stability characteristics of a typical tilt-wing V/STOL aircraft. Calculations have been made for the initial condition of steady level flight at wing incidences corresponding to speeds ranging from hovering to conventional forward flight. The results of the calculations have been compared with qualitative measurements of dynamic stability obtained during free-flight tests of a 1/9-scale model of the aircraft.

The results of the investigation indicated that the control-fixed motions of the aircraft without artificial stabilization in hovering flight would be dominated by an unstable oscillation similar to that displayed by most helicopters. As the transition to conventional forward flight progressed, stability characteristics were encountered in which aperiodic divergent modes of motion, as well as unstable oscillations, were present. The conventional-aircraft short-period and phugoid oscillations began to appear at the high-speed end of the transition. In general, the analytical results agreed with the motions observed during the free-flight model tests. These results also indicated that the unstable oscillation occurring in the hovering and low-speed flight regions can be stabilized by the addition of a combination of pitch-rate and pitch-attitude stabilization, but that angle-of-attack stability must be increased if the aperiodic divergent modes of motion are to be made stable.

INTRODUCTION

A considerable amount of data relating to qualitative measurements of the dynamic stability characteristics of dynamically scaled models of tilt-wing V/STOL aircraft has been published by the National Aeronautics and Space Administration. (For examples, see refs. 1 to 3.) At the present time, however, there is a lack of detailed information on the modes of motion and on the effect of various stability derivatives on the stability characteristics of this type of aircraft. The deficiency has been due in large part to the

unavailability of representative values of the static and dynamic stability derivatives for V/STOL aircraft.

As the first step of a program to provide some basic detailed information regarding the dynamic stability characteristics of tilt-wing configurations, static and dynamic longitudinal stability derivatives were determined for a powered 1/9-scale model of a four-propeller tilt-wing V/STOL transport (ref. 4). Prior to the force tests, the model was flown in free-flight tests during which qualitative measurements were made of the control-fixed longitudinal motions at several speeds in the transition range (ref. 3). The experimentally determined values of the stability derivatives were the necessary inputs for an analytical investigation of dynamic stability, and the model flight tests provided data for purposes of correlation and validation. The present investigation was undertaken (1) to determine appropriate methods with which to analyze the longitudinal dynamics of tilt-wing vehicles, (2) to calculate the dynamic stability of a typical tilt-wing aircraft over the transition flight range, (3) to correlate the results of the calculations with those of the model free-flight tests, and (4) to determine the effects of the various static and dynamic stability derivatives on control-fixed dynamic stability.

SYMBOLS

All stability derivatives are presented with respect to the body system of axes shown in figure 1. Inasmuch as conventional nondimensional coefficients lose their significance and tend to become infinite as airspeed approaches zero, the stability derivatives are presented in dimensional form. The units used for the physical quantities in this paper are given both in the U.S. Customary Units and in the International System of Units (SI). Factors relating the two systems of units are given in reference 5.

A,B,C,D,E coefficients defined in appendix A

$\bar{c}$ mean aerodynamic chord, ft (m)

$C_{1/2}$ cycles required for oscillation to damp to one-half amplitude

C_2 cycles required for oscillation to double amplitude

F_X force along X body axis, lb (N)

F_Z force along Z body axis, lb (N)

g acceleration due to gravity, ft/sec^2 (m/sec^2)

i_t tail incidence, deg

i_w wing incidence, deg

I_Y moment of inertia about Y body axis, slug-ft^2 (kg-m^2)

$j = \sqrt{-1}$

l aircraft linear dimension, ft (m)

l_M model linear dimension, ft (m)

L_o value of lift for longitudinal acceleration equal to zero at an angle of attack of 0^o, lb (N)

m mass, slugs (kg)

M_Y pitching moment, ft-lb (m-N)

P period of oscillation, sec

q pitching velocity, rad/sec

q_∞ dynamic pressure, $\rho V^2/2$, lb/ft^2 (N/m^2)

s Laplace operator, $\sigma + j\omega$, 1/sec

S wing area, ft^2 (m^2)

$t_{1/2}$ time required for a mode of motion to damp to one-half amplitude, sec

t_2 time required for a mode of motion to double amplitude, sec

u,w perturbation velocities along X and Z body axes, ft/sec (m/sec)

U_o trim velocity, ft/sec (m/sec) or knots

$\left|\frac{w}{u}\right|$ ratio of amplitude of perturbation velocity along Z body axis to perturbation velocity along X body axis

$\left\lvert \frac{\theta}{u} \right\rvert$	ratio of amplitude of perturbation in pitch angle to perturbation velocity along X body axis, $\frac{\text{deg}}{\text{ft/sec}}$ $\left(\frac{\text{deg}}{\text{m/sec}}\right)$
V	velocity, ft/sec (m/sec)
ΔV	velocity increment, ft/sec (m/sec)
W/S	wing loading, lb/ft^2 (N/m^2)
X,Y,Z	body reference axes (fig. 1)
α	angle of attack, deg or rad
$\Delta\alpha$	increment of angle of attack, rad
γ	flight-path angle, positive for climb, rad
ζ	ratio of damping present in oscillatory mode of motion to value required for critical damping
θ	pitch angle, positive when nose is above horizon, deg or rad
λ	scale factor, l/l_M
ρ	air density, $slugs/ft^3$ (kg/m^3)
σ	real part of root of characteristic equation, 1/sec
ω	imaginary part of root of characteristic equation, rad/sec
ω_n	undamped natural frequency of oscillatory mode, rad/sec

Dimensional stability derivatives:

$$M_u = \frac{1}{I_Y}\frac{\partial M_Y}{\partial u} \qquad M_w = \frac{1}{I_Y}\frac{\partial M_Y}{\partial w} \qquad M_q = \frac{1}{I_Y}\frac{\partial M_Y}{\partial q}$$

$$M_\alpha = \frac{1}{I_Y}\frac{\partial M_Y}{\partial \alpha} \qquad M_\theta = \frac{1}{I_Y}\frac{\partial M_Y}{\partial \theta} \qquad M_{\dot{\alpha}} = \frac{1}{I_Y}\frac{\partial M_Y}{\partial \dot{\alpha}} \qquad M_{\dot{w}} = \frac{1}{I_Y}\frac{\partial M_Y}{\partial \dot{w}}$$

$$X_u = \frac{1}{m}\frac{\partial F_X}{\partial u} \qquad X_w = \frac{1}{m}\frac{\partial F_X}{\partial w} \qquad X_q = \frac{1}{m}\frac{\partial F_X}{\partial q}$$

$$Z_u = \frac{1}{m}\frac{\partial F_Z}{\partial u} \qquad Z_w = \frac{1}{m}\frac{\partial F_Z}{\partial w} \qquad Z_q = \frac{1}{m}\frac{\partial F_Z}{\partial q}$$

Dot over a symbol indicates a derivative with respect to time.

METHOD OF ANALYSIS

The initial phase of the study consisted of an analytical determination of the dynamic longitudinal stability characteristics of a typical tilt-wing V/STOL aircraft for level flight (values of α and γ initially equal to zero) at several values of wing incidence. A large part of the investigation was devoted to arriving at suitable methods of analysis – in particular, to a determination of whether the classical linearized, small-perturbation equations of motion normally used in conventional aircraft stability analysis would adequately describe the control-fixed motions of a tilt-wing vehicle. The validity of linear equations of motion when applied to tilt-wing aircraft might be questionable because (1) large-amplitude control-fixed motions are expected to occur for V/STOL aircraft (see refs. 1 to 3) and (2) aerodynamic nonlinearities have been reported for tilt-wing configurations over part of the transition flight range (see ref. 4). The classical approach is, of course, the simplest method of analyzing dynamic-stability problems. The results of the calculations made with the linear equations of motion were compared with the scaled-up results of the free-flight model tests to determine the validity of the calculations. In conjunction with the linear analysis, values of the various longitudinal stability derivatives appearing in the equations of motion were varied not only to determine which derivatives had significant effects on dynamic stability and must therefore be known with a reasonable degree of accuracy, but also to determine which derivatives were so insignificant that they could be neglected for purposes of analysis.

Description of Aircraft

The aircraft used for the calculations was a four-propeller, tilt-wing V/STOL transport and is believed to be typical of present-day flapped tilt-wing designs. A three-view sketch showing the more important dimensions is presented in figure 2. The configuration employed counterrotating propellers, which resulted in cancellation of the propulsive gyroscopic effects and, in turn, in uncoupling of the longitudinal and lateral equations of motion. The mass and geometric characteristics of the V/STOL transport are given in table I. The values were obtained by scaling up the corresponding values for the 1/9-scale model as measured during the free-flight tests of reference 3. Scaling factors used are given in table II. The horizontal and vertical locations of the center of gravity were assumed to vary with wing incidence angle in the same manner as those for the free-flight model; the variations are presented in figure 3. The configuration employed a full-span flap and an all-movable horizontal tail. These two surfaces were programed to deflect with wing incidence. The programed variations of the flap deflection and horizontal-tail incidence (identical to those of the free-flight model) are shown in figure 4 and are the same as those used in reference 4. Unbalanced pitching moments occurring with this particular programed variation were assumed to be trimmed by an auxiliary device (the free-flight model was trimmed with a jet-reaction type of control) with no resulting effect on the longitudinal stability derivatives.

The results of reference 4 indicate that the tail-incidence program used produced excessive values of tail incidence at the higher transition speeds – that is, large nose-down pitching moments were produced by the horizontal tail. This point should be kept in mind inasmuch as the tail-incidence program produced negative (statically destabilizing) values of the velocity stability derivative M_u. In other words, when the speed of the model was increased from the trim flight condition, the pitching-moment contribution of the jet-reaction-control trimmer remained unchanged, but the moment increment due to the horizontal tail became more negative. The result is that different trimming procedures for tilt-wing configurations may lead to completely different values of the longitudinal stability derivatives. For example, the velocity stability derivative M_u will vary at higher speeds, depending upon whether the vehicle is trimmed with the horizontal tail or another trimming device such as a tail rotor.

Correlation of the results of the present study with those of similar configurations (refs. 6 and 7, for example) was not attempted because of differences in tail-incidence programs and mass and inertial characteristics.

Stability Derivatives

The static-force-test data of reference 4 (obtained for conditions of constant power) were linearized by measuring representative slopes of the force and moment data plotted

as functions of angle of attack and velocity. Slopes were obtained for forward flight for each wing incidence at the power condition that gave zero net longitudinal force at an angle of attack of zero $\left(F_X = 0 \text{ at } \alpha = 0^o\right)$. The static stability derivatives were then expressed in terms of the perturbation velocities u and w by the approximate relations $\Delta V \approx u$ and $U_o \Delta\alpha \approx w$. The change of variables was desirable inasmuch as the values of the stability derivatives for hovering (where α is undefined) and for forward flight then become directly comparable. This procedure was not required for estimation of the derivatives for hovering flight inasmuch as the data presented in reference 4 were measured as direct functions of u. Values of the stability derivatives representing rate of change of vertical and horizontal forces with respect to the variables in the equations of motion were divided by the value of the model mass, whereas derivatives of pitching moment were divided by the model moment of inertia in pitch. The dimensional stability derivatives were then scaled up to full-scale values by multiplying the model values by the appropriate scaling factors given in table II. Multiplication of model values by the scaling factors results in no change in dynamic stability – that is, the model and aircraft have the same values for the nondimensional stability characteristics (for example, $C_{1/2}$ and ζ).

Several difficulties arose in the estimation of the stability derivatives. First, the results of reference 4 did not report data for the dynamic derivatives in hovering flight. Preliminary calculations indicated that the only dynamic derivative which could significantly affect the hovering dynamics was the damping-in-pitch derivative M_q. Unpublished forced oscillation tests subsequent to those of reference 4 indicated that the model had values of M_q equal to zero in hovering flight. The small value of the derivative was also confirmed by the results of damping-in-pitch tests made with a similar configuration, as reported in reference 6. For the foregoing reasons, the dynamic derivatives for hovering flight were assumed to have values of zero for the aircraft without artificial stabilization. A second difficulty which arose during the estimation of stability derivatives was that the vertical damping derivative Z_w was not measured during the model force tests. For hovering flight, the value of Z_w was also assumed to be equal to zero. This assumption was not a critical one for the dynamic-stability calculations because the vertical translatory mode of motion is normally uncoupled from an unstable oscillation involving horizontal translation and pitching motion which dominates the control-fixed motions in hovering flight (see refs. 1 to 3). Information regarding height control of hovering VTOL aircraft (where the value of Z_w may be relatively important) can be found in references 8 and 9. A third difficulty arose when the static-force-test data of reference 4 showed significant nonlinear variations of pitching moment with angle of attack for a wing incidence of 25^o. (The static-force-test data for this condition are presented in fig. 5 for reference.) For the trim condition $\left(L_o/q_\infty S = 7.0\right)$, the model was statically stable with respect to angle of attack (negative values of M_α) for small negative

angles of attack but was unstable (positive values of M_α) for small positive angles of attack. It might be expected that this nonlinearity would preclude the valid usage of linear equations for that particular wing incidence. In order to evaluate the validity of the linear equations, slopes were measured at both small values of positive and negative angles of attack. Two values of angle-of-attack stability were therefore obtained for $i_w = 25^o$. A final difficulty was that the nature of the forced oscillation tests of reference 4 led to dynamic-stability parameters that were combinations of stability derivatives due to pitch rate (q) and rate of change of angle of attack ($\dot{\alpha}$). For purposes of the calculations, the measured parameters were assumed to be due entirely to pitch rate (for example, the measured parameter $M_q + M_{\dot{\alpha}}$ was used as M_q).

The stability derivatives as determined by the foregoing methods and used in the calculations are presented in figure 6 and in table III.

Method and Scope of Calculations

Calculations were made to determine the longitudinal dynamic stability characteristics of the vehicle for level flight at wing incidence angles of 90^o (hovering), 65^o, 50^o, 25^o, and 10^o. The calculations were not intended to describe the motions of an accelerated transition in which the stability derivatives are functions of time. Instead, the investigation was made to determine the stability of the vehicle in steady flight at each value of wing incidence. Presented in figure 7 and table III are the full-scale trim velocities for the particular wing-incidence values. The linearized, small-perturbation equations of motion used for the calculations are given in appendix A. Further simplification of the equations for hovering flight is discussed in appendix B. The stability parameters obtained from the solutions of the linear equations were in the form of damping and periodic characteristics of the modes of motion. The damping characteristics included time to damp to one-half amplitude $(t_{1/2})$, damping ratio (ζ), and number of cycles required to damp to one-half amplitude $(C_{1/2})$. Positive values of these parameters indicate stability and negative values indicate dynamically unstable modes of motion. The periodic characteristics were the damped period (P) and the undamped natural frequency (ω_n) of oscillatory modes. Additional calculations were made to determine the general nature of the modes of motion as expressed by the amplitude ratio $\left|\frac{w}{u}\right|$. Small values of this parameter indicate modes of motion containing little change in angle of attack (for example, the conventional-aircraft phugoid oscillation). Large values indicate large variations in angle of attack (similar to the conventional-aircraft short-period oscillation).

In conjunction with the linear analysis, the root-locus technique of reference 10 was used to illustrate graphically the variation of the roots of the characteristic equation with changes in the various stability derivatives. This method presents the path, or locus,

of the solutions on the complex plane as the value of an individual stability derivative is varied. (Additional information on the application of the method can be found in ref. 11.) Presented in figure 8 are the features of the complex plane as applied to dynamic systems. For stability, all roots of the characteristic equation must have negative real parts (σ negative). This requirement means that for stability all roots must be located in the left half of the complex plane shown in figure 8. The imaginary axis (at $\sigma = 0$) is therefore a line of neutral dynamic stability for both real and complex roots. Lines representing constant values of time to halve (or double) amplitude are parallel to the imaginary axis (σ = Constant). Lines representing constant values of damped period are parallel to the real axis ($j\omega$ = Constant). Radial lines emanating from the origin represent constant values of damping ratio or cycles to halve (or double) amplitude (ω/σ = Constant). Circles with centers at the origin represent lines of constant undamped natural frequency $\left(\sqrt{\sigma^2 + \omega^2} = \text{Constant}\right)$.

Although calculations were made for the nonlinear condition of $i_w = 25^o$, the results were rather meaningless for the present configuration inasmuch as the motion of the vehicle depended on the direction of the disturbance. Additional calculations were therefore made by using the basic force-test data of figure 5 in a digital computer program. This program utilized complete nonlinear equations of motion which were solved by numerical methods to produce representative time histories of motions obtained at $i_w = 25^o$.

RESULTS AND DISCUSSION

Calculated Stability of Aircraft

Hovering flight.- The roots describing the modes of motion on the complex plane are plotted in figure 9 for hovering flight. A real root with a value equal to zero ($\sigma = 0$) representing the neutral stability of the vertical motion of the vehicle appears at the origin. A negative (stable) real root associated with an aperiodic mode involving both horizontal translation and pitching motion is shown on the negative real axis. The additional roots were a complex pair whose real part σ was positive (unstable). As pointed out in appendix B, the oscillation involved both fore-and-aft motions and pitch-attitude changes. After a disturbance from hovering flight, the damped aperiodic mode would rapidly subside and the dynamic stability of the vehicle would be dominated by the unstable oscillation.

The calculated stability characteristics of the aperiodic and oscillatory modes corresponding to the roots are presented in table IV. The vertical translatory mode is neutrally stable $\left(t_{1/2} = \infty\right)$, because the derivative Z_w was assumed to have a value of zero, as previously discussed. The other aperiodic mode is relatively highly damped

$(t_{1/2} = 0.8$ sec$)$. The oscillation is unstable in terms of time required to double amplitude $(t_2 = 2.4$ sec$)$ with a moderately long period (P = 9.7 sec). These modes of motion are similar to those displayed by most helicopters in hovering flight, although the oscillation is more unstable for the tilt-wing aircraft. For example, the basic helicopter used in the investigation of reference 12 also possessed an aperiodic mode $(t_{1/2} = 0.31$ sec$)$ and an unstable oscillation $(P = 8.9$ sec, $t_2 = 6.6$ sec$)$ in hovering flight. The point to be inferred is that dynamic instability can be tolerated for tilt-wing aircraft in hovering flight if they are operated in the same manner as helicopters. The fact that complete dynamic stability is not required for satisfactory handling qualities is also demonstrated by conventional aircraft with unstable phugoid or spiral modes of motion.

Transition flight.- The data of table IV show that as the wing incidence is reduced from 90^o to 65^o, the most noticeable change from the stability characteristics of hovering flight is the appearance of an unstable aperiodic mode of motion. Analysis revealed that this instability of the vehicle was a result of angle-of-attack instability $(\text{positive values of } M_w)$ as indicated by the data of figure 6(a). The data of table IV also show that as the wing incidence was reduced from 90^o to 65^o, the unstable oscillation increased in period (from P = 9.68 sec to P = 14.11 sec) and was less unstable in terms of time required to double amplitude ($t_2 = 4.29$ sec). The stable aperiodic mode for $i_w = 65^o$ had about the same value of $t_{1/2}$ as for hovering flight. The data of table IV also indicate that the aperiodic modes of motion involve larger angle-of-attack changes $\left(\left|\frac{w}{u}\right|\right)$ than does the oscillatory mode.

As the transition progresses and the wing incidence is reduced to 50^o, the larger value of angle-of-attack instability (see fig. 6(a)) results in greater instability of the unstable aperiodic mode. The oscillation is still unstable and continues to increase both in period (P = 19.40 sec) and in time required to double amplitude ($t_2 = 16.50$ sec). The general nature of the aperiodic and oscillatory modes for $i_w = 50^o$ is apparent in that the aperiodic modes contain larger changes in angle of attack and pitch angle than does the oscillatory mode.

Further reduction in wing incidence to 25^o results in the aerodynamic nonlinearities previously discussed. The results of calculations from the linearized values of the static data based on positive and negative angle-of-attack disturbances indicate that the motion initiated by positive angle-of-attack disturbances would be dominated by an aperiodic divergence (primarily in angle of attack and pitch angle) caused by the static instability with respect to angle of attack. For negative angle-of-attack disturbances, on the other hand, two oscillatory modes similar to the classical phugoid and short-period oscillations are present. The results of the linearized calculations for negative angle-of-attack disturbances are meaningless in that, as the aircraft angle of attack returns to the trim

condition and overshoots, the static instability will prevail – that is, the aircraft will always diverge in a nose-up direction. The results of additional calculations made by using automatic-computing equipment and the basic nonlinear data of figure 5 are presented in figure 10. These data are time histories of the motions resulting from initial angle-of-attack disturbances of 5° and -5°. The motions for positive angle-of-attack disturbances show simply that the model diverges. For negative angle-of-attack disturbances, the vehicle initially tends to return to the trim condition; but, as the angle of attack overshoots, the model diverges as it did for the positive disturbance. The results for $i_w = 25^{\circ}$ indicate that the classical linearized equations of motion are not applicable to some of the normal flight conditions of tilt-wing aircraft.

For the lowest value of wing incidence of this investigation ($i_w = 10^{\circ}$), the results show a highly damped relatively short period oscillation, a stable aperiodic mode, and an unstable aperiodic mode. The amplitude ratios presented in table IV for $i_w = 10^{\circ}$ indicate that the oscillation primarily involved changes in angle of attack and pitch angle $\left(\text{large values of } \left|\frac{w}{u}\right| \text{ and } \left|\frac{\theta}{u}\right|\right)$ whereas the aperiodic modes primarily involved large changes in forward speed $\left(\text{relatively small values of } \left|\frac{w}{u}\right| \text{ and } \left|\frac{\theta}{u}\right|\right)$. The instability of one of the aperiodic modes was found to be a result of static instability of the aircraft. In this connection, it should be pointed out that the static stability of a V/STOL aircraft is dependent on factors other than angle-of-attack stability. For this particular wing incidence, the vehicle was statically stable with respect to angle of attack (see fig. 6(a)) but the tail-incidence program led to negative (destabilizing) values of the velocity stability derivative M_u. An inspection of the coefficient E of the quartic characteristic equation in appendix A reveals that both angle-of-attack stability (M_w) and velocity stability (M_u) can determine the static stability of the aircraft. (A negative sign of the coefficient E indicates static instability.) For $i_w = 10^{\circ}$, the unstable value of velocity stability was large enough to cause static instability of the aircraft. These results are believed to be further substantiated by the free-flight tests of a tilt-wing model as reported in reference 2. The model used for the investigation of reference 2 also had excessive values of tail incidence at high transition speeds. In spite of the fact that force tests showed the model to have static stability with respect to angle of attack, control-fixed motions were observed to be aperiodic divergences. Such motions might, of course, be taken to be out-of-trim flight conditions. Although no measurements were made of the velocity stability derivative, it is believed that a condition existed similar to that for the present configuration – that is, instability of the model due to excessive values of tail incidence.

The root locations of the equations of motion for transition flight (except for the nonlinear condition of $i_w = 25^{\circ}$) are plotted on the complex plane in figure 11. The

values of the mode ratios $\left|\frac{w}{u}\right|$ and $\left|\frac{\theta}{u}\right|$ given in table IV, together with the data of figure 11, reveal that as the wing incidence is progressively reduced from 90^{o}, the complex roots describing the unstable oscillation of hovering flight move to the left (less unstable) and closer to the origin (increase in period). Then, these complex roots separate into two real roots defining one stable and one unstable aperiodic mode. The negative real root of hovering flight ($i_W = 90^{o}$) has approximately the same value at the low transition speeds ($i_W = 65^{o}$ and 50^{o}) but combines with the other (unstable) real root to form the damped short-period oscillation at $i_W = 10^{o}$.

The roots describing the dynamic stability of the present vehicle are seen to follow a distinct path as the transition to forward flight progresses (fig. 11). The real aperiodic modes of hovering flight become the conventional-aircraft short-period oscillation of forward flight whereas the unstable oscillation of hovering flight becomes the phugoid oscillation of forward flight; although, for this configuration, the phugoid oscillation is broken down into two real roots because of static instability with respect to speed. Additional calculations for $i_W = 10^{o}$ with a value of $M_u = 0$ show that a phugoid oscillation results with little change in the short-period mode. In a subsequent section of this paper, the path of the roots is shown to depend heavily on the relative values of M_W and M_u. For example, the hovering flight oscillation became the short-period oscillation in forward flight during flight tests of an experimental tilt-wing aircraft (see ref. 13).

Correlation of Calculated and Experimental Results

As previously stated, the model used in the measurement of the stability derivatives had undergone a series of free-flight tests during which measurements were made of observed control-fixed longitudinal dynamic stability characteristics. A complete description of the free-flight technique used for the tests is given in reference 3. A photograph of the 1/9-scale model in free flight in the Langley full-scale tunnel is presented as figure 12. The dynamic-stability measurements consisted of time histories obtained from motion-picture records of control-fixed motions occurring after random atmospheric disturbances from trim flight conditions. No attempt was made to match calculated time histories because of the random nature of the disturbance input; instead, the basic character of the motions in terms of period and damping are compared. Motions measured using the free-flight model technique are those which would be seen by an observer flying alongside the model at the steady trim speed U_o. Typical control-fixed longitudinal motions of this type, based on scaled-up model values obtained during the tests, are presented for several wing incidence angles in figure 13. The model motions are seen to agree with the results of the calculations (table IV) in an overall sense in that the model had an unstable oscillation in hovering flight and became less unstable at high transition speeds. The calculated period and damping of the oscillatory mode of hovering

flight (P = 9.68 sec, t_2 = 2.38 sec) agree well with the scaled-up model values (P = 10.4 sec, t_2 = 2.5 sec). As the transition to forward flight progressed and the wing incidence was reduced to 65°, the oscillation became longer in period (P = 12.4 sec for scaled-up model value and 14.11 sec for calculated value) than that for hovering flight. Because of the unstable oscillation, the aperiodic divergence could not be confirmed, but the model certainly seemed to be simply diverging in a nose-down sense at the end of the record. As wing incidence was further reduced to 25°, an unusually long period "oscillation" was noted for an initially nose-down motion. This flight condition emphasizes the fact that although the time histories of figure 13 are informative, any inspection of limited samples of the model motions under certain circumstances may lead to erroneous conclusions regarding the dynamic stability of free-flight models. This is particularly true for conditions involving very nonlinear and unsymmetrical aerodynamic characteristics. The previously discussed aerodynamic nonlinearity for $i_w = 25°$ was not known at the time the free-flight tests were conducted; as a result, the time history is based on nose-down motion. Additional examination of motion pictures taken during the flights revealed that the model would not oscillate when disturbed in a nose-up sense but would pitch up, as indicated in figure 10. These motions were regarded as a result of out-of-trim conditions during the free-flight tests. At the lowest wing incidence of the investigation (10°), the model motions observed during the free-flight tests were a short-period oscillation in angle of attack and pitch angle and a lightly damped phugoid oscillation or aperiodic divergence in displacement.

The fact that the results of the calculations are in fairly good agreement with the motions observed during the free-flight tests indicates that linearized stability calculations can be applied to tilt-wing aircraft for most flight conditions. More sophisticated time-consuming means of analysis may be required for certain flight conditions in which nonlinear and unsymmetrical aerodynamic characteristics prevail.

Effect of Individual Stability Derivatives on Dynamic Stability

The values of the various longitudinal static and dynamic stability derivatives were varied with the use of the root-locus method in order to determine the effect of the individual stability derivatives on dynamic stability. Calculations similar to those previously discussed were also made in which the basic values of the stability derivatives were doubled and halved in order to illustrate the magnitude of each derivative at various points along the locus. The derivatives were varied at all wing incidences for which the dynamic stability calculations previously discussed were made except $i_w = 25°$ (the nonlinear case). Since preliminary calculations indicated that the dynamic derivatives X_q, X_w, and Z_q were of negligible importance throughout the range of flight conditions investigated, the effects of these derivatives were not studied in detail. Consequently, results are not presented for these particular derivatives. The following table presents

an index to the figures in which the root-locus results are presented for the various derivatives:

Derivative	Figure		
Hovering flight, $i_w = 90^o$			
M_u	14		
X_u	15		
M_q and M_θ	16		
Transition flight			
	$i_w = 65^o$	$i_w = 50^o$	$i_w = 10^o$
X_u	17	23	29
Z_u	18	24	30
Z_w	19	25	31
M_u	20	26	32
M_w	21	27	33
M_q and M_θ	22	28	34

Hovering flight.- The locations of the roots presented in figure 14 for the various values of M_u indicate that the roots of the characteristic equation for hovering flight are relatively sensitive to changes in velocity stability. Increases in M_u lead to a more unstable oscillation with a corresponding decrease in period. It is interesting to note that the oscillation becomes more unstable in terms of time required to double amplitude (that is, σ becomes more positive) but the instability remains about constant in terms of number of cycles required to double amplitude ($\sigma/\omega \approx$ Constant). The locations of the roots presented in figure 15 show that although negative increases in X_u tend to make the modes of motion less unstable, the roots are relatively insensitive to changes in this derivative. Figure 16 shows the location of the roots representing the oscillation for pitch-rate stabilization ($M_\theta = 0$, $M_q = -2$ per rad-sec), pitch-attitude stabilization ($M_\theta = -1$ per rad-sec^2, $M_q = 0$), and various ratios of pitch-attitude stabilization to pitch-rate stabilization. With the addition of pitch-rate stabilization only ($M_\theta/M_q = 0$), the unstable oscillation can be made stable, but the vehicle response to control inputs will be sluggish. For the case of artificial stabilization in attitude alone ($M_\theta/M_q = \infty$), the frequency of the oscillation is increased with little change in the damping characteristics. The most effective means of stabilizing the unstable oscillation is through use of artificial stabilization in the form of a combination of pitch-rate (q) stabilization and pitch-attitude (θ) stabilization.

The unstable oscillation of hovering flight has not been of concern to pilots of V/STOL aircraft when flying in weather conditions where visual motion cues are available inasmuch as the pilot will add the rate and attitude stabilization necessary to stabilize the aircraft. Some difficulties, however, may arise during hovering flight when using instrument references only. Significant improvements in handling qualities were obtained by use of artificial stabilization during the flight tests of reference 7. In any event, at least artificial pitch-rate stabilization would probably be required for satisfactory handling qualities for this particular configuration.

Transition flight.- The root-locus plots presented in figures 17 to 22 for $i_w = 65^o$ show that the stability of the oscillatory mode is very sensitive to changes in M_u, M_q, and M_θ and relatively insensitive to changes in X_u and Z_u. The unstable oscillation could be made stable by the addition of artificial stabilization in M_q or M_θ. The unstable aperiodic mode is most sensitive to changes in the stability derivatives Z_w and M_w because of the relatively large angle-of-attack content in that mode for this low-speed transition flight region (see table IV).

The data presented in figures 23 to 28 for $i_w = 50^o$ indicate that the aircraft dynamic stability characteristics are sensitive to changes in all the stability derivatives except X_u and Z_w. The unstable oscillation is again stabilized by the addition of pitch-attitude or pitch-rate stabilization. The only stability derivative for which changes can stabilize the aperiodic divergence without destabilizing the oscillatory mode is M_w (fig. 27).

For $i_w = 10^o$, the root-locus plots shown in figures 29 to 34 indicate that the stability derivatives are beginning to assume the relative importance normally associated with conventional aircraft stability derivatives. For example, negative increases in Z_w tend to add damping to the short-period mode (fig. 31), negative increases in M_w tend to increase the frequency of the short-period oscillation (fig. 33), and negative increases in damping in pitch (M_q) increase the damping of the short-period mode with little effect on the phugoid roots (fig. 34). The unstable aperiodic mode of the basic configuration may be stabilized by a negative increase in Z_u (fig. 30), a reduction in the negative value of Z_w (fig. 31), a reduction in the negative value of M_u (fig. 32), or a negative increase in M_w (fig. 33).

SUMMARY OF RESULTS

The results of an analytical investigation of the dynamic longitudinal stability of a tilt-wing V/STOL aircraft may be summarized as follows:

1. The results of the calculations using the classical linearized equations of motion agree with the results of free-flight tests of a 1/9-scale model of the vehicle. However,

the linearized equations may not be applicable to the tilt-wing aircraft for some flight conditions in which aerodynamic nonlinearities are present.

2. The control-fixed longitudinal motions of the tilt-wing aircraft without artificial stabilization in hovering flight were dominated by an unstable oscillation similar to that displayed by most helicopters. As the transition to conventional forward flight progressed, stability characteristics were encountered in which aperiodic divergent modes of motion, as well as unstable oscillations, were present. The conventional-aircraft short-period and phugoid oscillations began to appear at the high-speed end of the transition.

3. The unstable oscillation occurring in the hovering and low-speed flight regions can be stabilized by the addition of a combination of pitch-rate and pitch-attitude stabilization, but angle-of-attack stability must be increased if the aperiodic divergences are to be made stable.

Langley Research Center,
National Aeronautics and Space Administration,
Langley Station, Hampton, Va., June 23, 1967,
721-01-00-26-23.

APPENDIX A

EQUATIONS OF MOTION

The linearized, small-perturbation equations of motion for fuselage-level horizontal flight (ref. 11), referred to a body system of axes (fig. 1), may be expressed as follows:

Vertical force:

$$-Z_u u + (s - Z_w)w - (U_o + Z_q)s\theta = 0 \tag{A1}$$

Longitudinal force:

$$(s - X_u)u - X_w w + (g - X_q s)\theta = 0 \tag{A2}$$

Pitching moment:

$$-M_u u - (M_w + M_{\dot{w}} s)w + (s^2 - M_q s - M_\theta)\theta = 0 \tag{A3}$$

For nontrivial solutions, s must be a root of the characteristic equation

$$As^4 + Bs^3 + Cs^2 + Ds + E = 0 \tag{A4}$$

where

$A = 1$

$B = M_{\dot{w}}(-Z_q - U_o) - M_q - X_u - Z_w$

$C = M_{\dot{w}}(U_o X_u + Z_q X_u - X_q Z_u) - M_w(U_o + Z_q) + X_u(Z_w + M_q) - X_q M_u - M_\theta + M_q Z_w - Z_u X_w$

$D = M_{\dot{w}}(gZ_u) + X_q(M_u Z_w - Z_u M_w) + Z_q(X_u M_w - M_u X_w) + M_\theta(Z_w + X_u) + M_w(U_o X_u)$
$+ X_w(M_q Z_u - U_o M_u) + gM_u - M_q Z_w X_u$

$E = g(Z_u M_w - M_u Z_w) + M_\theta(Z_u X_w - Z_w X_u)$

The damping and period of a mode of motion, in seconds, are given by the equations $t_{1/2} = -\frac{0.693}{\sigma}$ and $P = \frac{2\pi}{\omega}$, respectively, where σ and ω are the real and imaginary parts of the root of the characteristic equation. Additional stability characteristics may be obtained by the following relations:

$$C_{1/2} = t_{1/2}/P \qquad \omega_n = \sqrt{\sigma^2 + \omega^2} \qquad \zeta = \frac{-\sigma}{\omega_n}$$

APPENDIX B

SIMPLIFIED EQUATIONS OF MOTION FOR HOVERING FLIGHT

Considerable simplification of the general equations of motion given in appendix A can be made for hovering flight. Inasmuch as the stability derivatives X_w, M_w, and $M_{\dot{w}}$ will usually be negligible, the vertical-force equation becomes uncoupled from the horizontal-force and pitching-moment equations. The resulting characteristic equation is

$$(s - Z_w)\left[s^3 - (X_u + M_q)s^2 + (X_u M_q - M_u X_q - M_\theta)s + (X_u M_\theta + M_u g)\right] = 0 \qquad \text{(B1)}$$

As a consequence of the uncoupling of the vertical degree of freedom, one root (equal in value to Z_w) is immediately known. The remaining cubic describes the oscillation involving the fore-and-aft and pitch degrees of freedom.

REFERENCES

1. Tosti, Louis P.: Flight Investigation of Stability and Control Characteristics of a 1/8-Scale Model of a Tilt-Wing Vertical-Take-Off-and-Landing Airplane. NASA TN D-45, 1960.

2. Newsom, William A., Jr.: Flight Investigation of the Longitudinal Stability and Control Characteristics of a Four-Propeller Tilt-Wing VTOL Model With a Programed Flap. NASA TN D-1390, 1962.

3. Newsom, William A.; and Kirby, Robert H.: Flight Investigation of Stability and Control Characteristics of a 1/9-Scale Model of a Four-Propeller Tilt-Wing V/STOL Transport. NASA TN D-2443, 1964.

4. Chambers, Joseph R.; and Grafton, Sue B.: Static and Dynamic Longitudinal Stability Derivatives of a Powered 1/9-Scale Model of a Tilt-Wing V/STOL Transport. NASA TN D-3591, 1966.

5. Mechtly, E. A.: The International System of Units – Physical Constants and Conversion Factors. NASA SP-7012, 1964.

6. Curtiss, H. C., Jr.; Putman, W. F.; and Lebacqz, J. V.: An Experimental Investigation of the Longitudinal Dynamic Stability Characteristics of a Four Propeller Tilt-Wing VTOL Model at High Wing Incidences. Rept. No. 774 (Contract DA 44-177-AMC-8(T)), Dept. Aerospace Mech. Sci., Princeton Univ., Apr. 1966.

7. Ransome, Robin K.; and Jones, Gay E.: XC-142A V/STOL Transport Tri-Service Limited Category I Evaluation. FTC-TR-65-27, U.S. Air Force, Jan. 1966. (Available from DDC as AD 477 084.)

8. Garren, John F., Jr.; and Assadourian, Arthur: VTOL Height-Control Requirements In Hovering as Determined From Motion Simulator Study. NASA TN D-1488, 1962.

9. Gerdes, Ronald M.: A Piloted Motion Simulator Investigation of VTOL Height-Control Requirements. NASA TN D-2451, 1964.

10. Evans, Walter R.: Control-System Dynamics. McGraw-Hill Book Co., Inc., New York, 1954.

11. Seckel, Edward: Stability and Control of Airplanes and Helicopters. Academic Press, Inc., c.1964.

12. Seckel, E.; Traybar, J. J.; and Miller, G. E.: Longitudinal Handling Qualities for Hovering. Rept. No. 594 (Contract DA 44-177-TC-524), Dept. Aeron. Eng., Princeton Univ., Dec. 1961.

13. Pegg, Robert J.: Summary of Flight-Test Results of the VZ-2 Tilt-Wing Aircraft. NASA TN D-989, 1962.

TABLE I.- MASS AND GEOMETRIC CHARACTERISTICS OF THE V/STOL TRANSPORT

Gross weight, lb (N)	52 000 (231 307)
Moment of inertia in pitch, slug-ft^2 (kg-m^2)	205 000 (277 940)
Wing loading, lb/ft^2 (N/m^2)	97.2 (4 654)
Fuselage:	
Length, ft (m)	50.0 (15.2)
Cross-sectional area, maximum, ft^2 (m^2)	81.8 (7.6)
Height, ft (m)	12.2 (3.7)
Width, ft (m)	9.1 (2.8)
Wing:	
Area, ft^2 (m^2)	534.4 (49.6)
Span, ft (m)	67.5 (20.6)
Aspect ratio	8.53
Mean aerodynamic chord, ft (m)	8.07 (2.5)
Airfoil section	NACA 63_3-318
Tip chord, ft (m)	6.0 (1.8)
Root chord, ft (m)	9.8 (2.9)
Taper ratio	0.61
Sweepback of quarter chord, deg	4.13
Dihedral angle, deg	-2.12
Pivot location, percent root chord	42.5
Aileron, each:	
Chord, percent wing chord	25
Area, ft^2 (m^2)	31.1 (2.9)
Flap, each:	
Type	Double slotted
Chord, percent wing chord	47
Span	Full
Slat, each:	
Inboard, 0.45 wing semispan to 0.69 wing semispan	Chord, 0.20 wing chord inboard to 0.10 wing chord outboard
Outboard, 0.85 wing semispan to 1.00 wing semispan	Chord, 0.10 wing chord full length

TABLE I.- MASS AND GEOMETRIC CHARACTERISTICS

OF THE V/STOL TRANSPORT – Concluded

Vertical tail:	
Area, ft^2 (m^2)	130.0 (12.1)
Span, ft (m)	15.6 (4.8)
Aspect ratio	1.87
Airfoil section:	
Root	NACA 0018
Tip	NACA 0012
Tip chord, ft (m)	3.3 (1.0)
Root chord, ft (m)	13.3 (4.1)
Taper ratio	0.25
Sweepback of quarter chord, deg	26
Rudder:	
Tip chord, ft (m)	1.1 (0.3)
Root chord, ft (m)	3.8 (1.2)
Tail length, center of gravity to 0.25 mean aerodynamic chord, ft (m)	21.4 (6.5)
Horizontal tail:	
Area, ft^2 (m^2)	170.9 (15.9)
Aspect ratio	5.68
Airfoil section:	
Root	NACA 0015
Tip	NACA 0012
Tip chord, ft (m)	3.5 (1.1)
Root chord, ft (m)	7.0 (2.1)
Span, ft (m)	31.14 (9.5)
Taper ratio	0.50
Sweepback of quarter chord, deg	9.50
Mean aerodynamic chord, ft (m)	5.5 (1.7)
Tail length, center of gravity to 0.25 mean aerodynamic chord, ft (m)	24.8 (7.6)
Propellers:	
Main:	
Number of blades	4
Diameter, ft (m)	15.5 (4.7)
Tail:	
Number of blades	3
Diameter, ft (m)	8.0 (2.4)
Moment arm, wing pivot to rotor center, ft (m)	32.0 (9.8)

TABLE II.- SCALING FACTORS

$$\left[\text{To scale model values up to full-scale values, } \lambda = \frac{l}{l_M}\right]$$

Dimensional and mass properties	
To scale	Multiply by
Linear acceleration	1
Length	λ
Area	λ^2
Mass	λ^3
Force	λ^3
Moment	λ^4
Moment of inertia	λ^5
Linear velocity	$\lambda^{1/2}$
Time	$\lambda^{1/2}$
Angular velocity	$\lambda^{-1/2}$
Angular acceleration	λ^{-1}

Stability derivatives	
To scale	Multiply by
M_α	λ^{-1}
X_u, Z_u, X_w, Z_w	$\lambda^{-1/2}$
M_u, M_w	$\lambda^{-3/2}$
X_q, Z_q	$\lambda^{1/2}$
M_q	$\lambda^{-1/2}$
M_θ	λ^{-1}

TABLE III.- STABILITY DERIVATIVES

[All values are full scale]

(a) U.S. Customary Units

i_w, deg	U_o, ft/sec	X_u, per sec	X_w, per sec	X_q, ft/sec-rad	Z_u, per sec	Z_w, per sec	Z_q, ft/sec-rad	M_u, per ft-sec	M_w, per ft-sec	M_q, per rad-sec
90	0	-0.2855	0	0	0	0	0	0.0137	0	0
65	43.5	-.1848	0	-1.5426	-.1549	0	-3.6420	.0061	.0027	-.1940
50	51.9	-.1218	.1420	-2.7290	-.1759	-.0355	-4.3470	.0046	.0073	-.2235
25 (Nose up)	108.3	-.1058	.1531	.2031	-.1905	-.0681	-6.6030	-.0012	.0037	-.3553
25 (Nose down)	108.3	-.1058	.1531	.2031	-.1905	-.0681	-6.6030	-.0012	-.0011	-.3553
10	165.6	-.1189	.0445	.4548	-.2463	-.4230	-1.7190	-.0027	-.0032	-.7213

(b) SI Units

i_w, deg	U_o, m/sec	X_u, per sec	X_w, per sec	X_q, m/sec-rad	Z_u, per sec	Z_w, per sec	Z_q, m/sec-rad	M_u, per m-sec	M_w, per m-sec	M_q, per rad-sec
90	0	-0.2855	0	0	0	0	0	0.0449	0	0
65	13.3	-.1848	0	-.4702	-.1549	0	-1.1101	.0200	.0089	-.1940
50	15.8	-.1218	.1420	-.8318	-.1759	-.0355	-1.3250	.0151	.0240	-.2235
25 (Nose up)	33.0	-.1058	.1531	.0619	-.1905	-.0681	-2.0126	-.0039	.0121	-.3553
25 (Nose down)	33.0	-.1058	.1531	.0619	-.1905	-.0681	-2.0126	-.0039	-.0036	-.3553
10	50.5	-.1189	.0445	.1386	-.2463	-.4230	-.5240	-.0089	-.0105	-.7213

TABLE IV.- SUMMARY OF RESULTS FOR BASIC AIRCRAFT

i_w, deg	Mode	σ	ω	$t_{1/2}$, sec (*)	P, sec	$C_{1/2}$ (*)	ω_n	ζ (*)	$\left\|\frac{w}{u}\right\|$	$\left\|\frac{\theta}{u}\right\|$ deg ft/sec	$\left\|\frac{\theta}{u}\right\|$ deg m/sec
90	Oscillatory	0.29	±0.65	-2.38	9.68	-0.246	0.711	-0.410	0	1.55	5.09
	Aperiodic	0	0	∞					∞	----	----
	Aperiodic	-.87	0	.80					0	1.04	3.41
65	Oscillatory	0.16	±0.44	-4.29	14.11	-0.304	0.474	-0.341	0.59	0.99	3.25
	Aperiodic	.08	0	-8.99					2.33	.46	1.51
	Aperiodic	-.78	0	.89					.96	1.09	3.58
50	Oscillatory	0.04	±0.32	-16.50	19.39	-0.851	0.327	-0.129	0.41	0.69	2.26
	Aperiodic	.39	0	-1.77					1.33	1.21	3.97
	Aperiodic	-.86	0	.81					1.88	1.92	6.30
25	Oscillatory	-0.09	±0.24	8.09	26.67	0.303	0.251	0.342	0.41	0.38	1.25
(Nose up)	Aperiodic	.48	0	-1.45					3.43	1.99	6.53
	Aperiodic	-.84	0	.83					5.81	2.87	9.42
25	Oscillatory	-0.28	±0.36	2.48	17.57	0.141	0.454	0.616	2.52	1.33	4.36
(Nose down)	Oscillatory	.01	±.14	-46.70	44.91	-1.040	.141	-.105	1.40	.59	1.94
10	Oscillatory	-0.60	±0.75	1.15	8.42	0.137	0.959	0.628	7.29	2.05	6.73
	Aperiodic	.09	0	-7.96					.68	.42	1.38
	Aperiodic	-.15	0	4.74					.86	.02	.07

*Negative signs indicate unstable modes of motion. For example, if $t_{1/2} = -2.38$, then $t_2 = 2.38$.

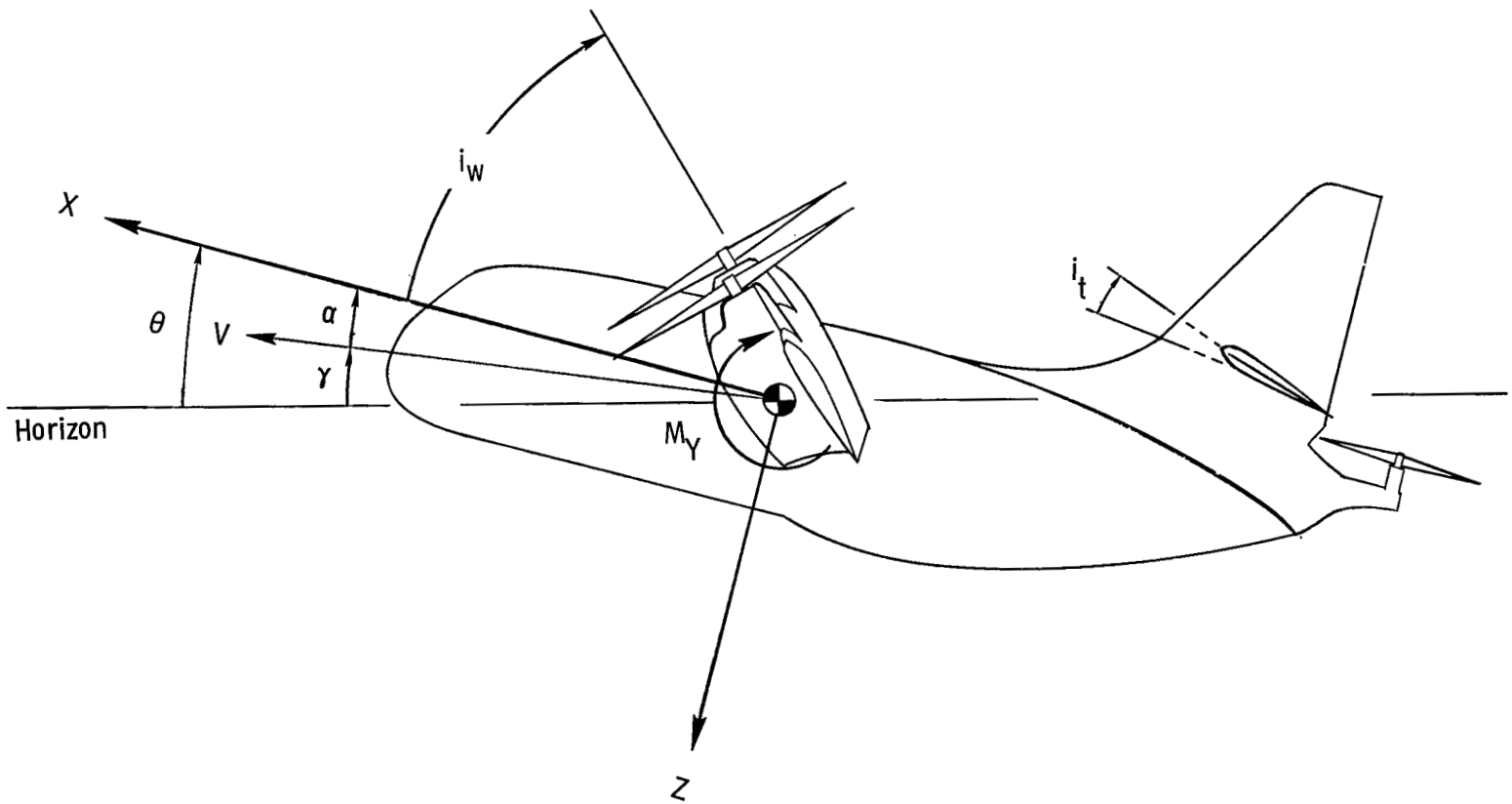

Figure 1.- The body system of axes.

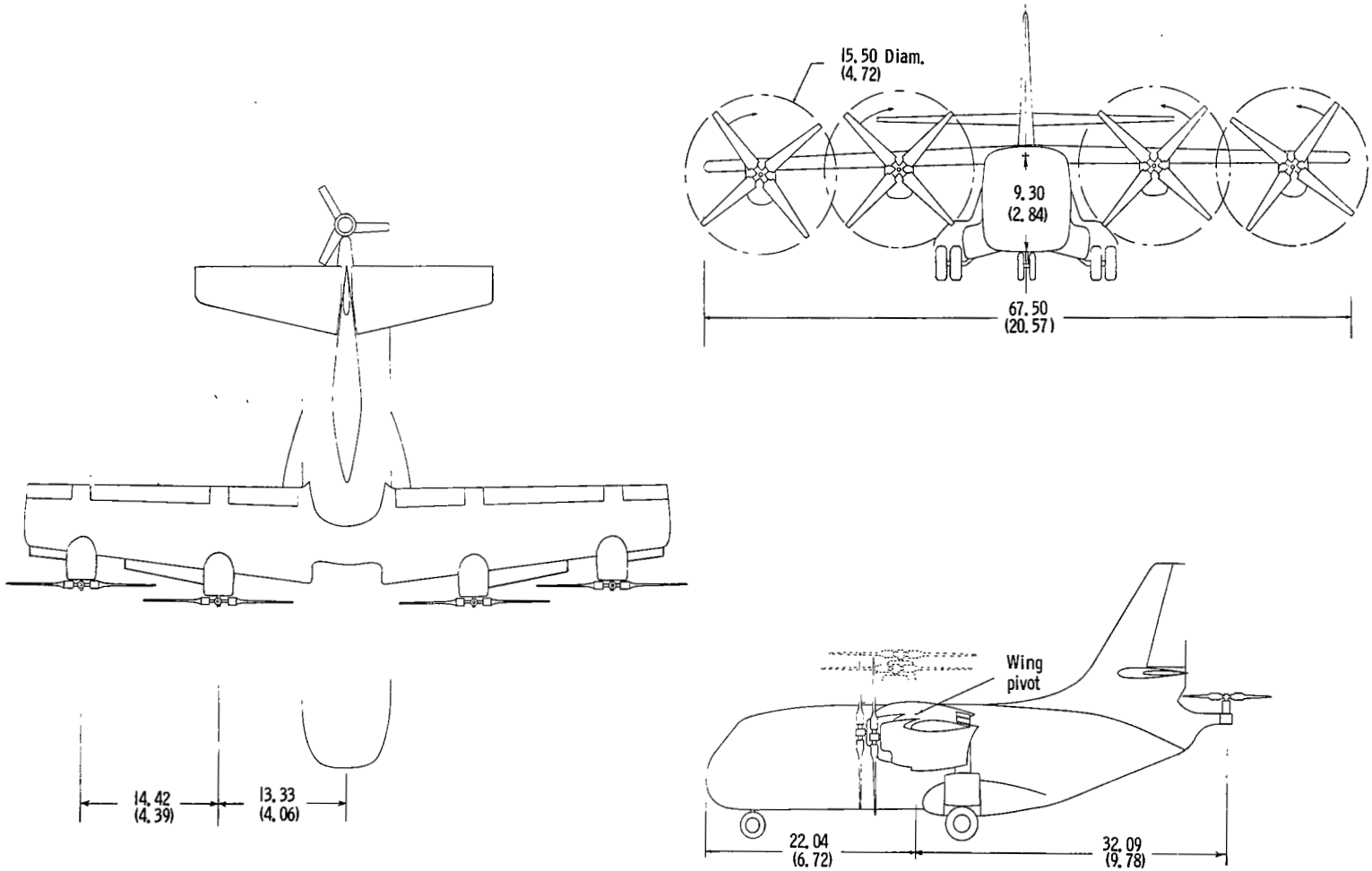

Figure 2.- Three-view drawing of the tilt-wing transport. Dimensions are given in feet and parenthetically in meters.

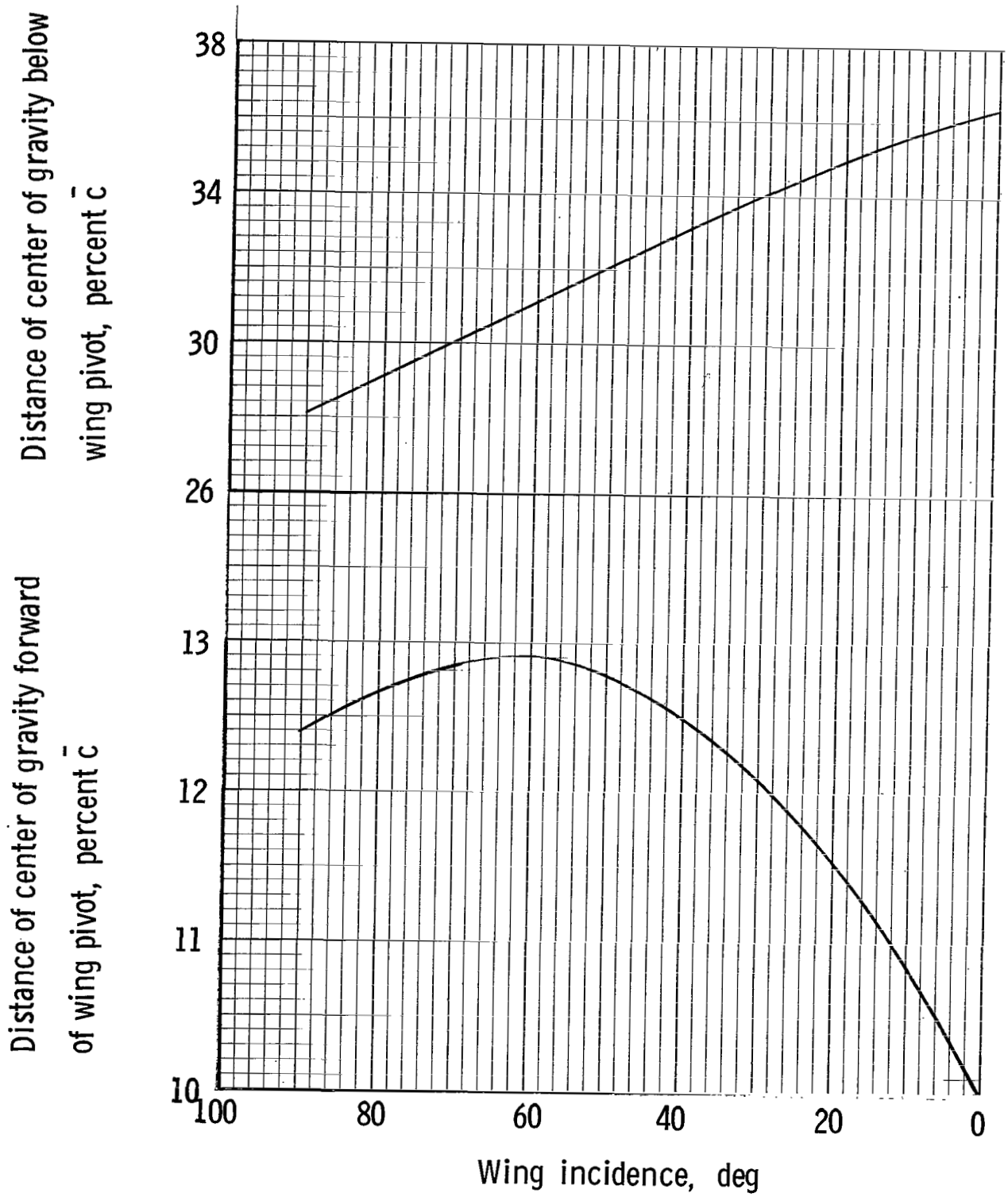

Figure 3.- Variation of the horizontal and vertical center-of-gravity locations with wing incidence.

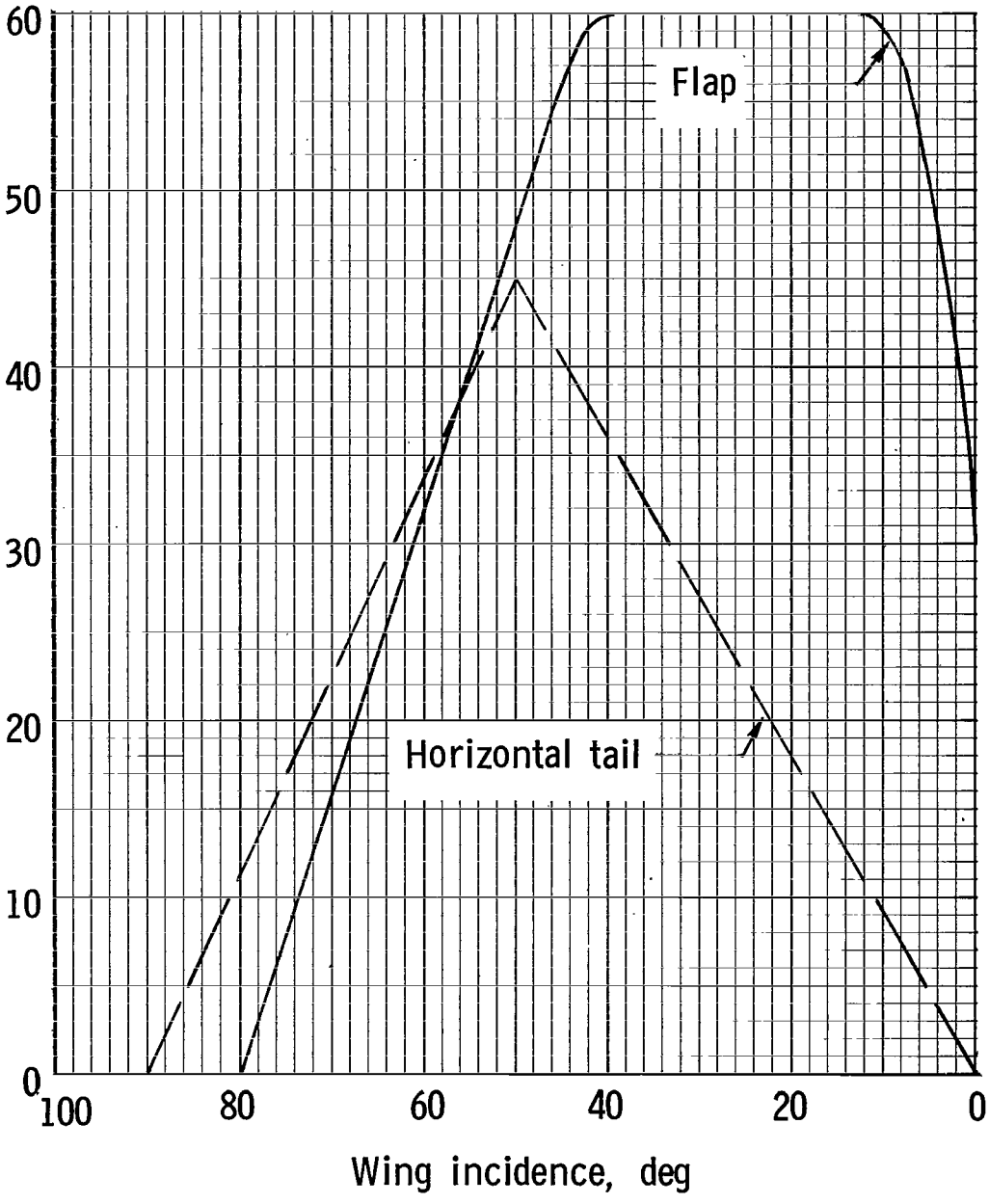

Figure 4.- Variation of flap deflection and horizontal-tail incidence with wing incidence.

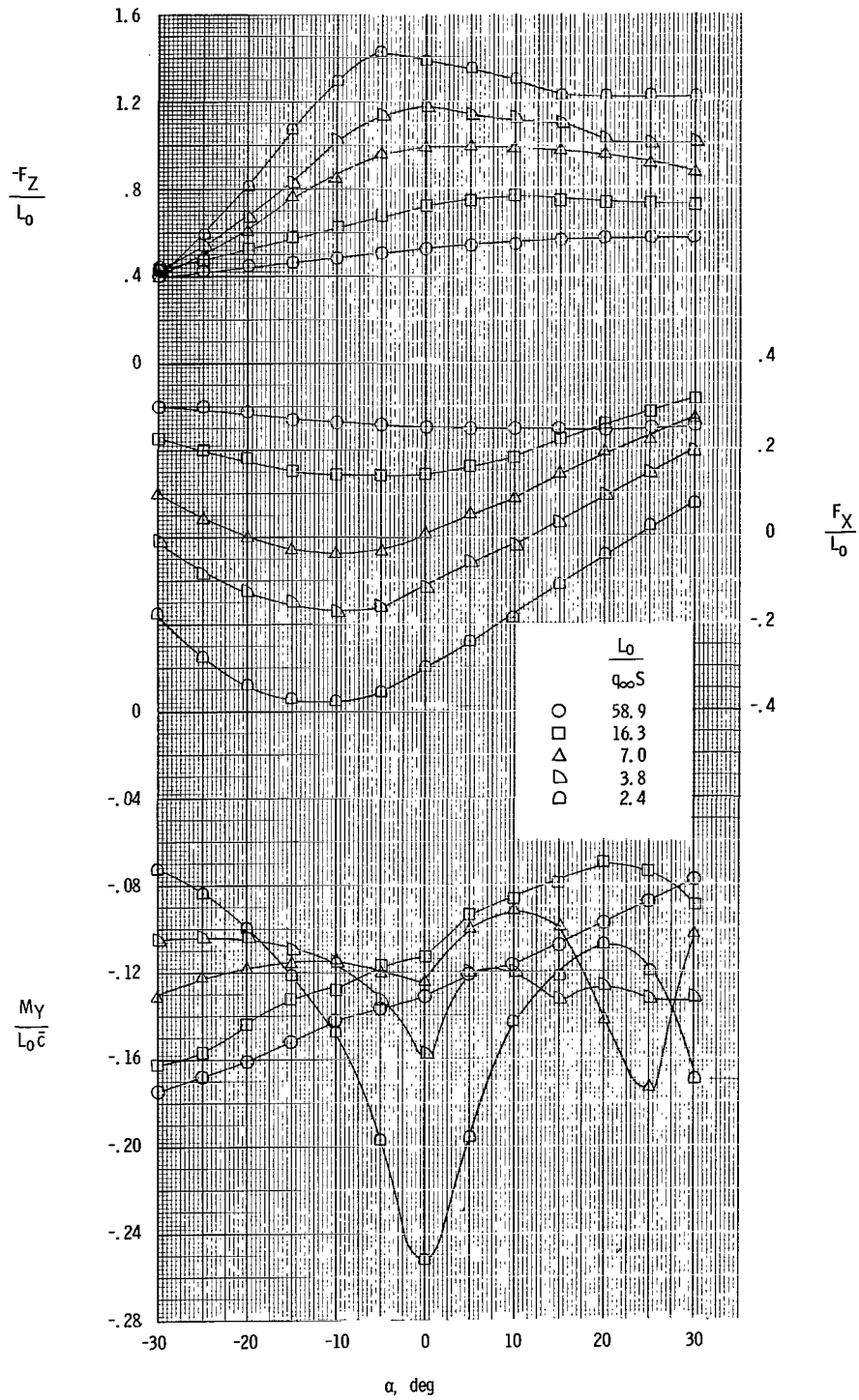

Figure 5.- Variation of forces and moments with angle of attack of the 1/9-scale model. $i_w = 25^0$; $i_t = 23^0$. (Figure from ref. 4.)

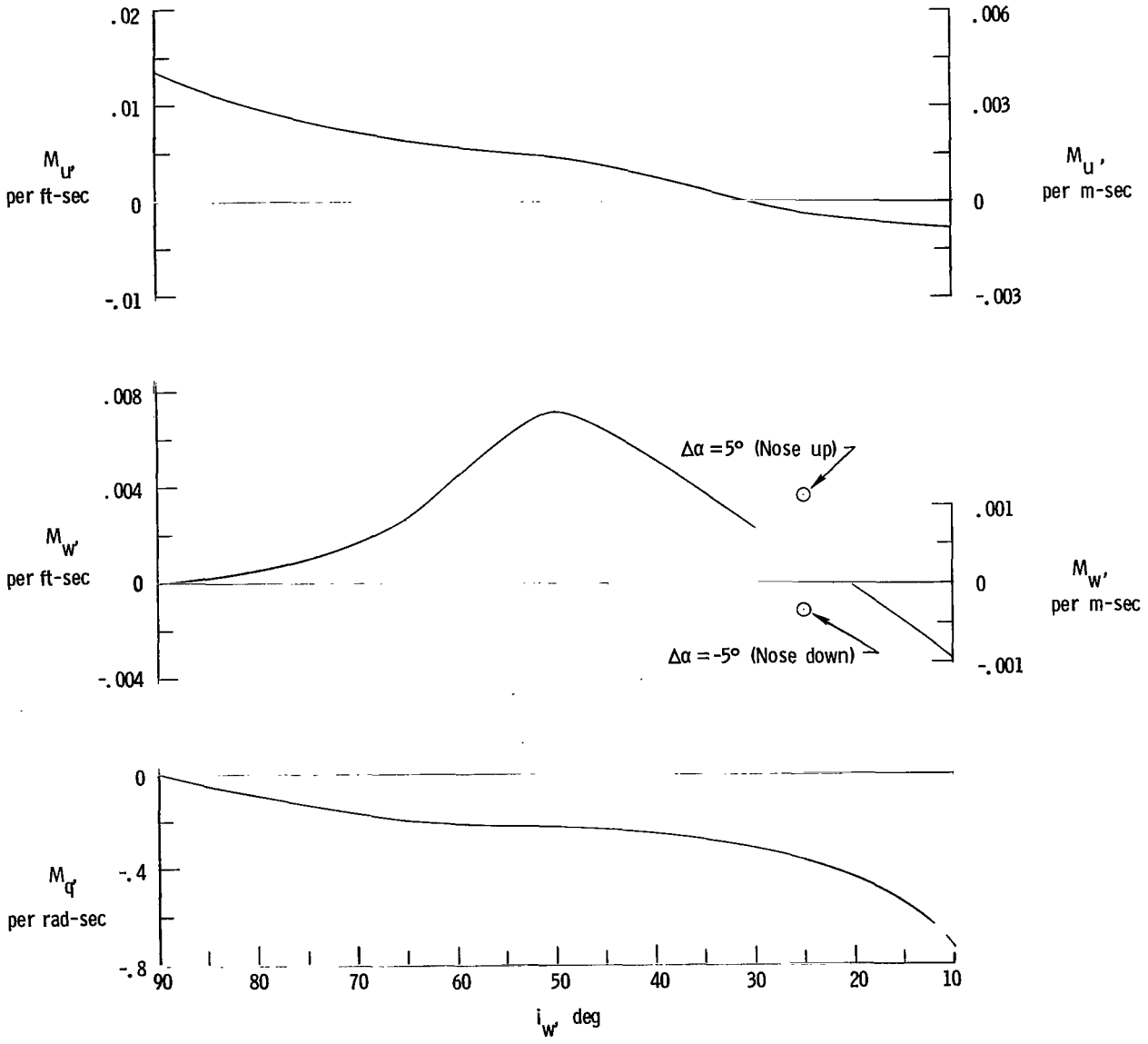

(a) Pitching-moment derivatives.

Figure 6.- Stability derivatives used in the calculations (full-scale values).

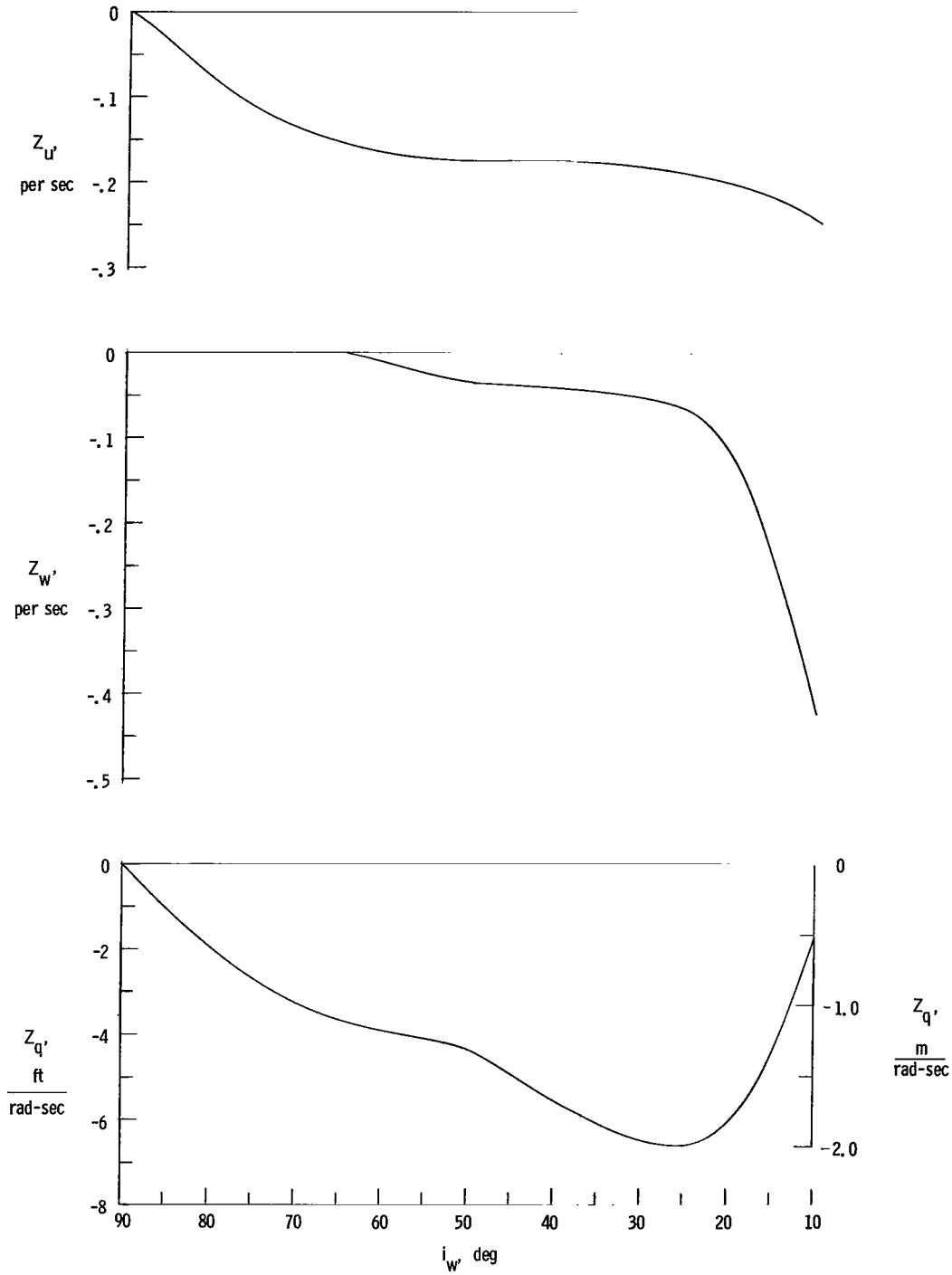

(b) Vertical-force derivatives.

Figure 6.- Continued.

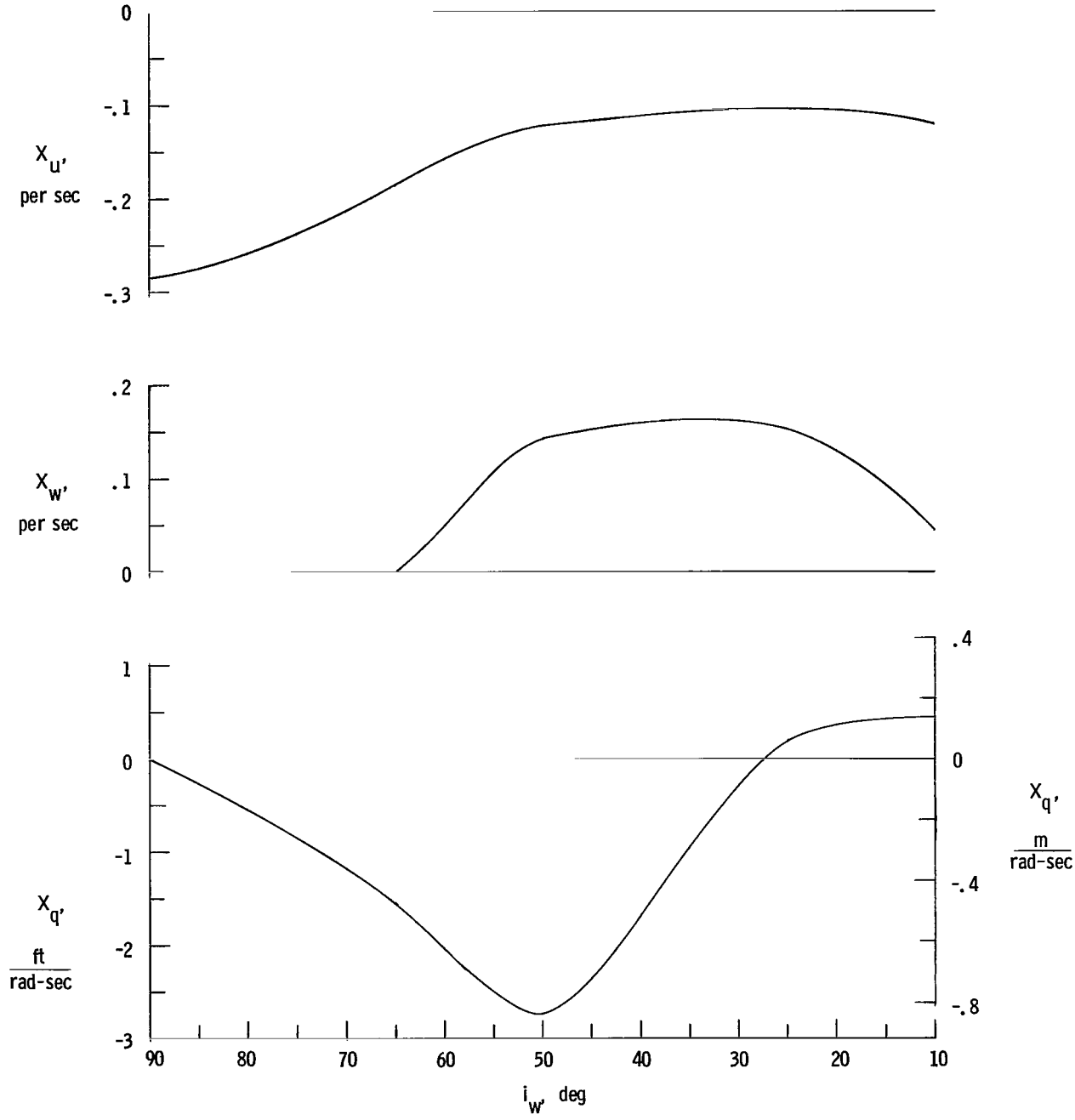

(c) Longitudinal-force derivatives.

Figure 6.- Concluded.

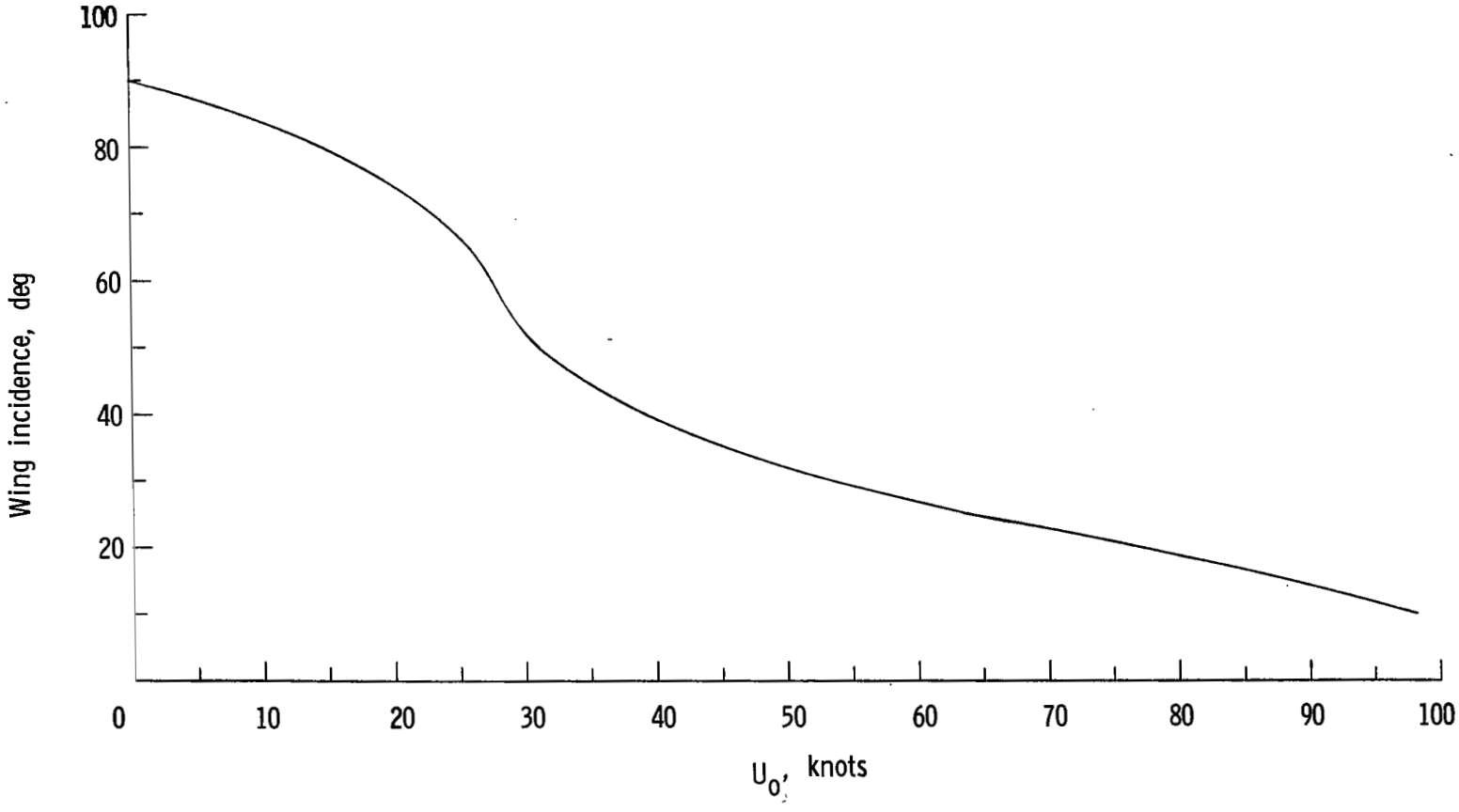

Figure 7.- Variation of trim velocity with wing incidence angle. W/S = 97.2 lb/ft^2 (4654 N/m^2).

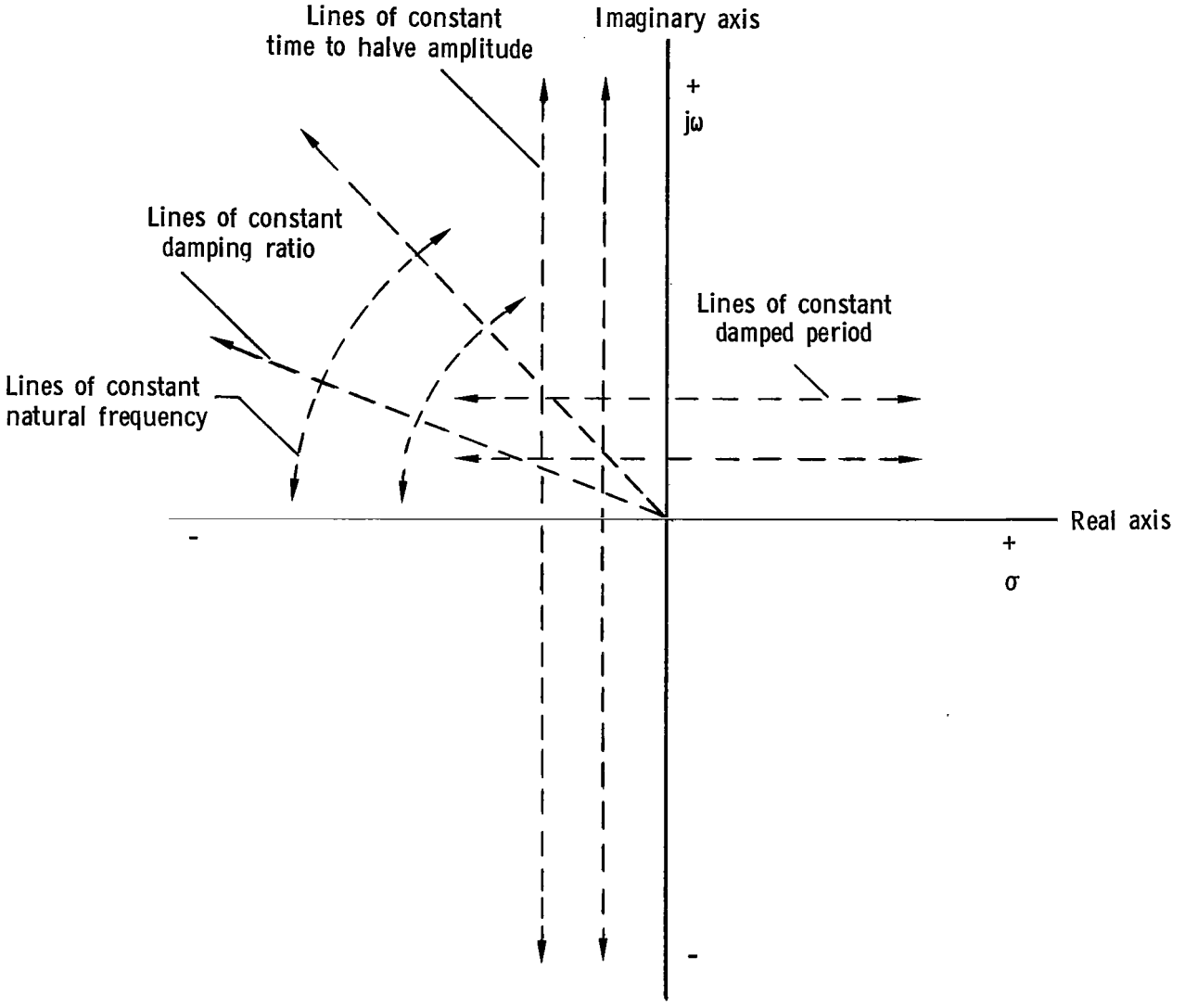

Figure 8.- Features of the complex plane as applied to dynamic systems.

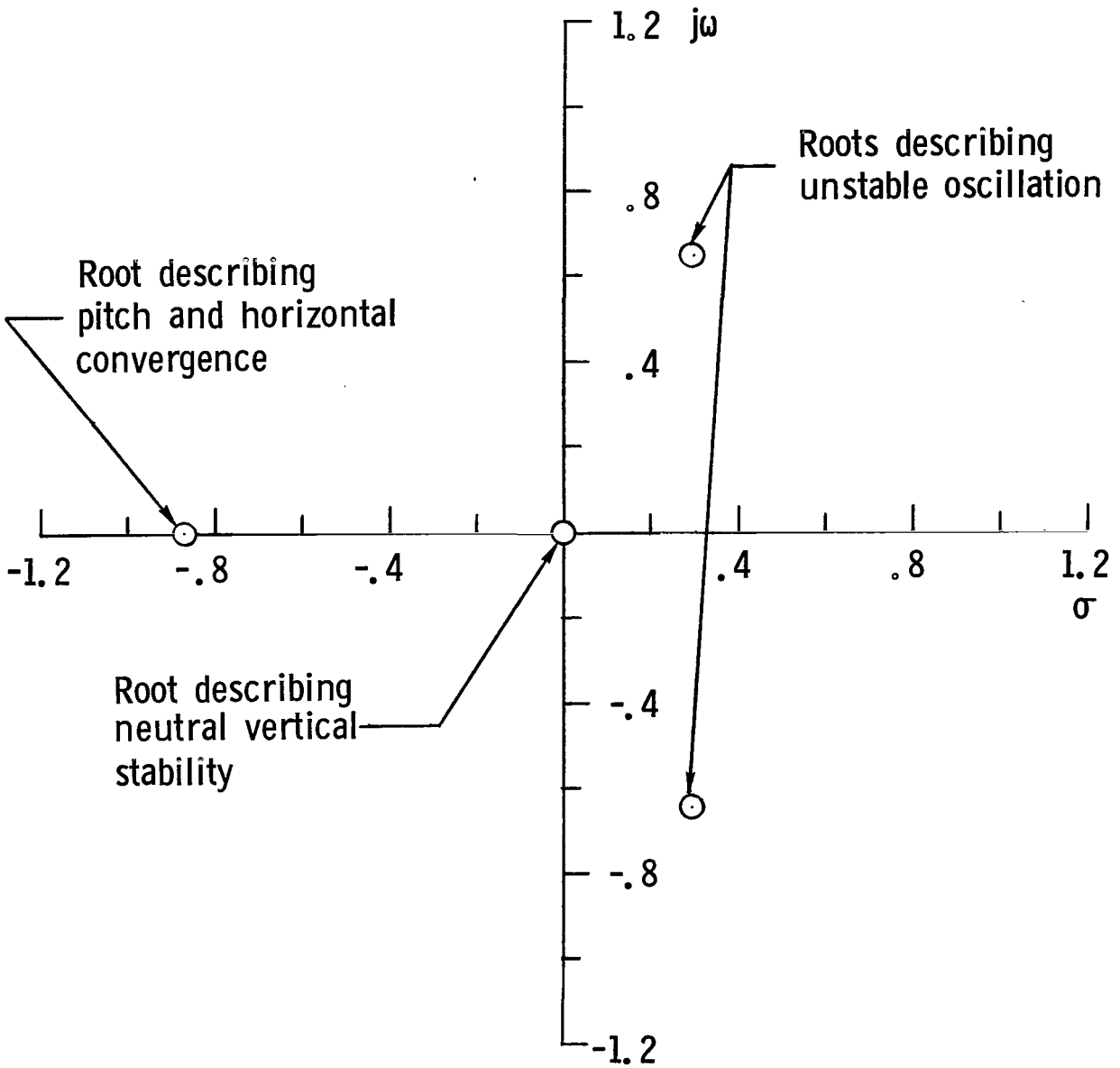

Figure 9.- Location of the roots on the complex plane for hovering flight.

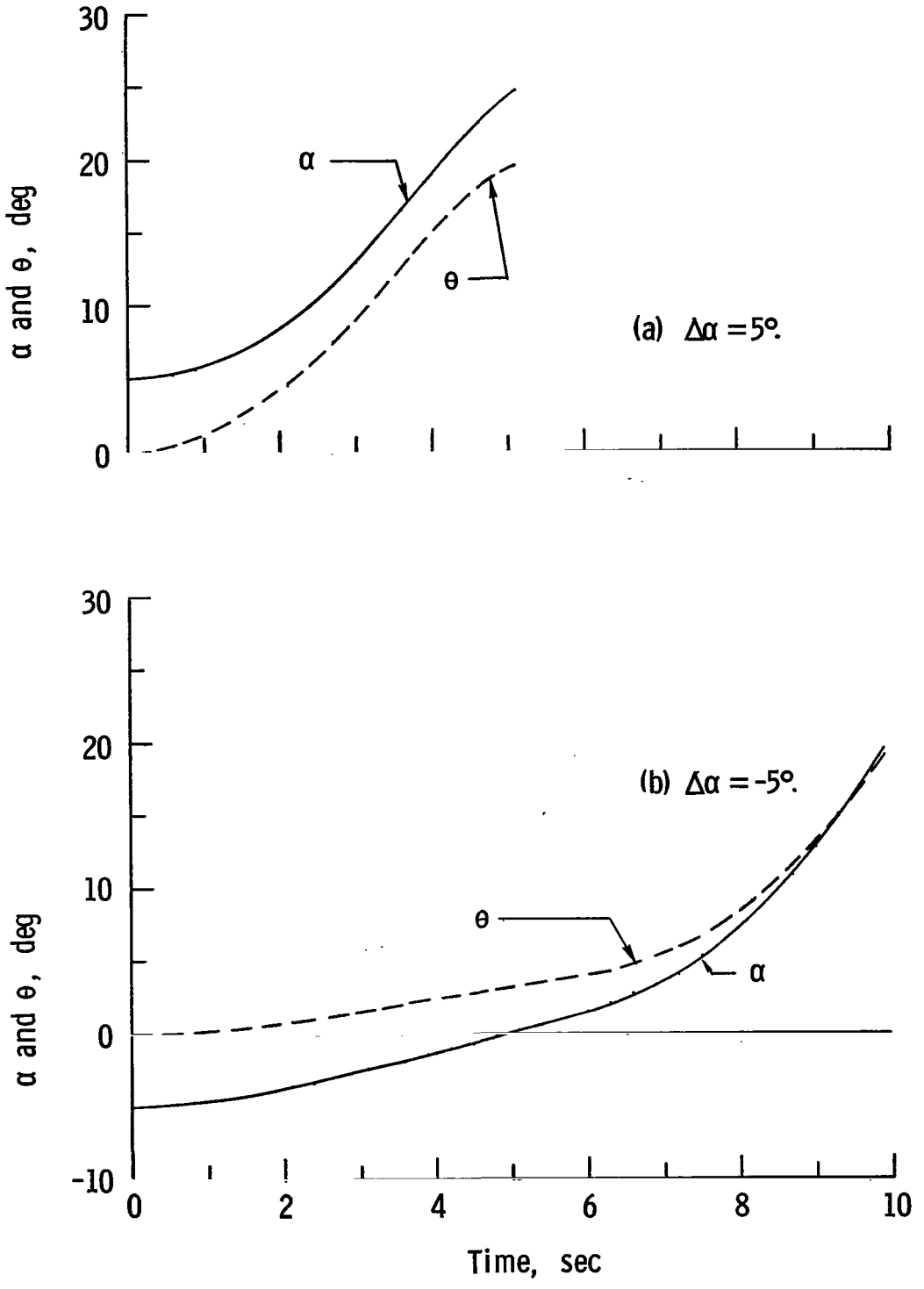

Figure 10.- Calculated time histories of motions at $i_w = 25^0$ showing dependence of dynamic characteristics on initial disturbance.

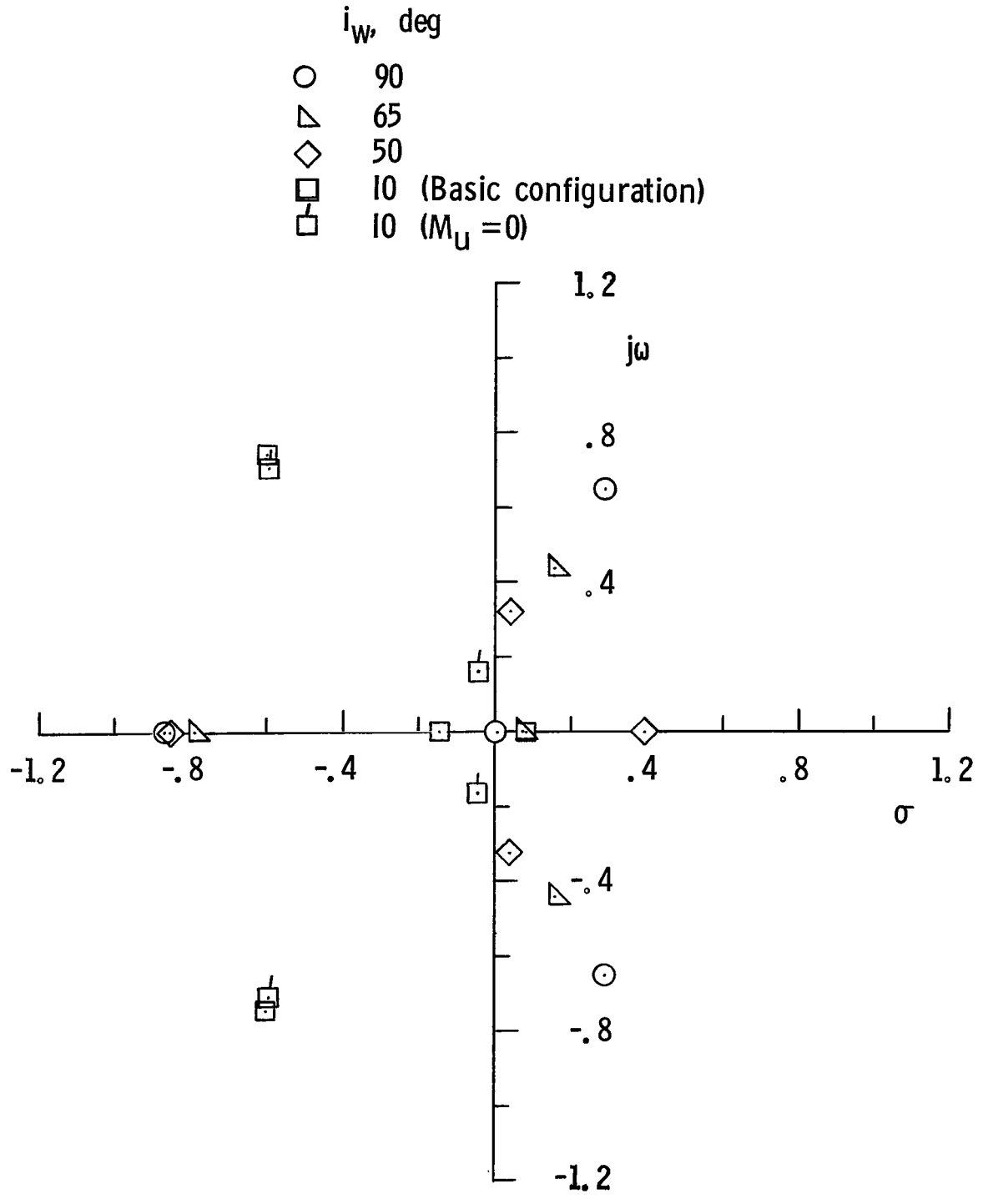

Figure 11.- Effect of wing incidence on the root locations on the complex plane. Level flight; $\alpha = 0^0$.

Figure 12.- Photograph of the 1/9-scale model in free flight.

L-63-8475

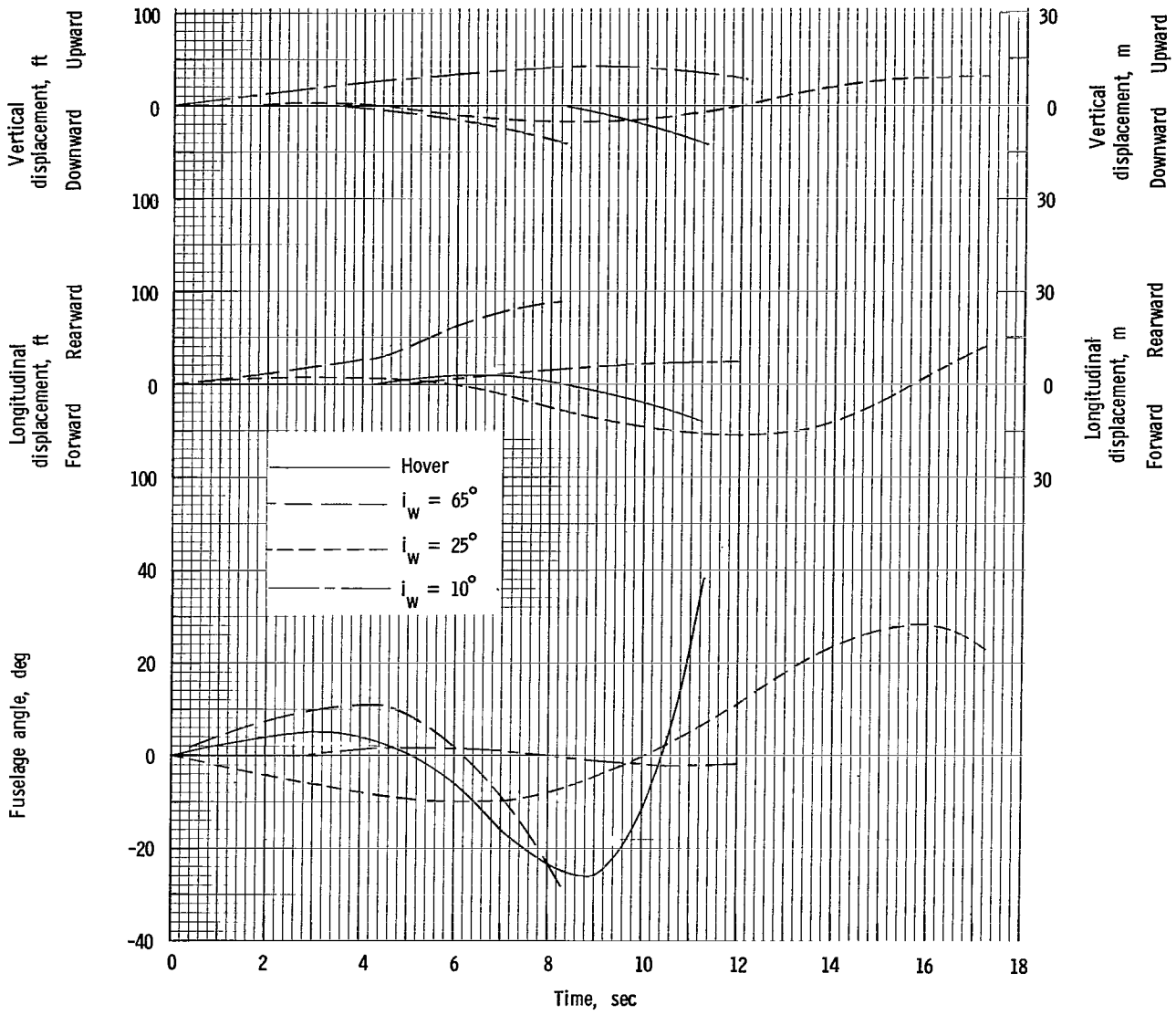

Figure 13.- Control-fixed longitudinal motions of the tilt-wing aircraft based on scaled-up results of the 1/9-scale model tests.

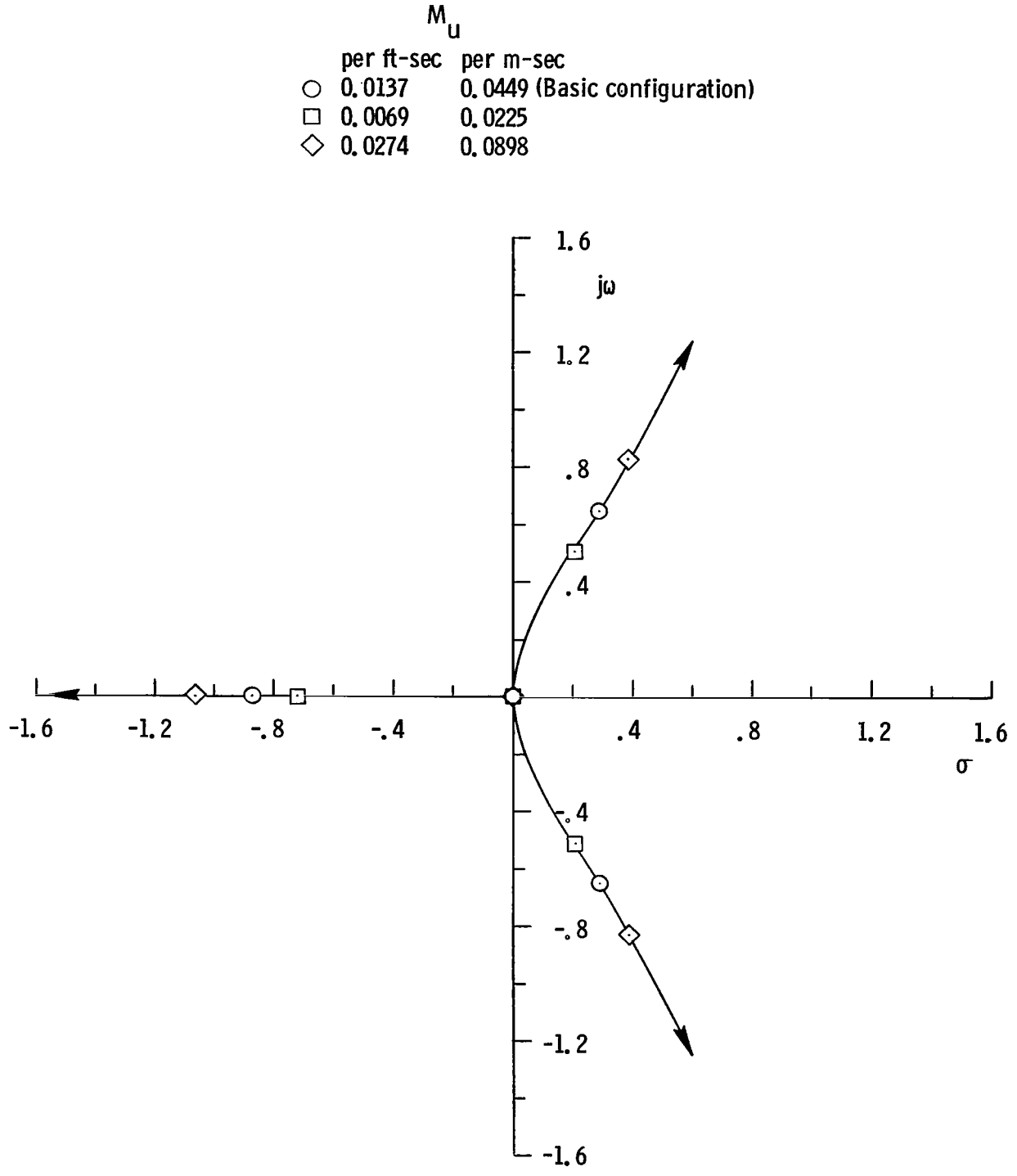

Figure 14.- Root locus for M_u. Hovering flight.

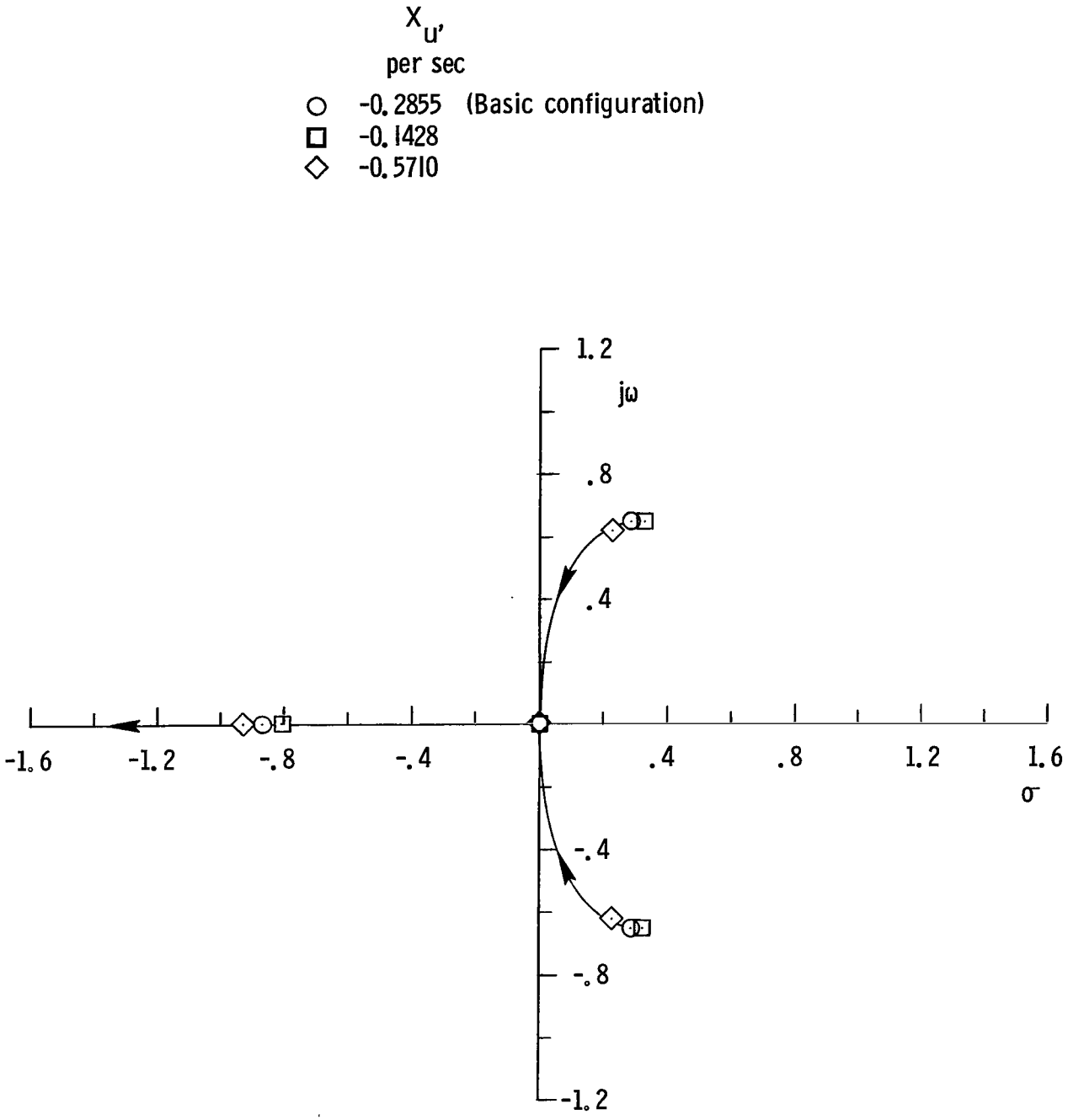

Figure 15.- Root locus for X_u. Hovering flight.

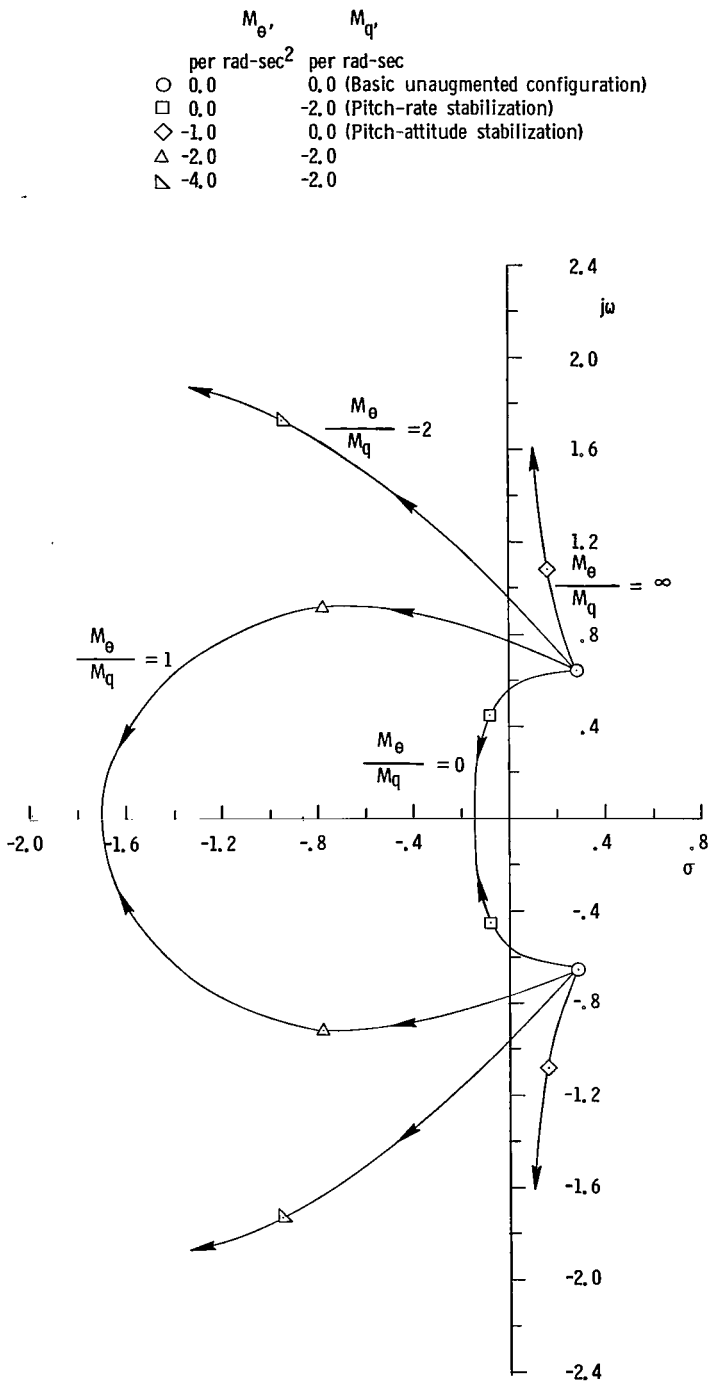

Figure 16.- Root locus for M_θ and M_q. Hovering flight. (Unit for M_θ/M_q is per sec.)

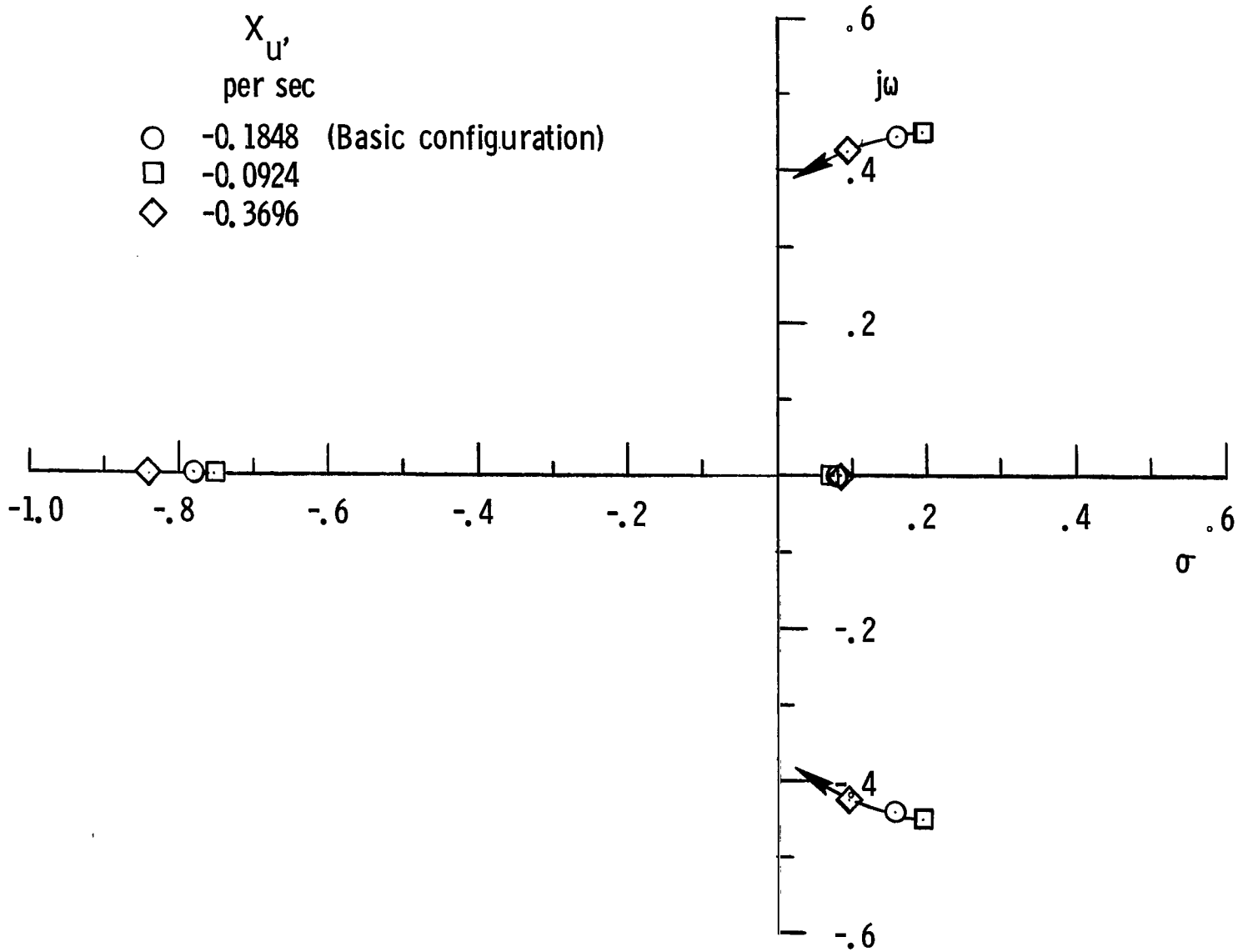

Figure 17.- Root locus for X_u. $i_w = 65^0$.

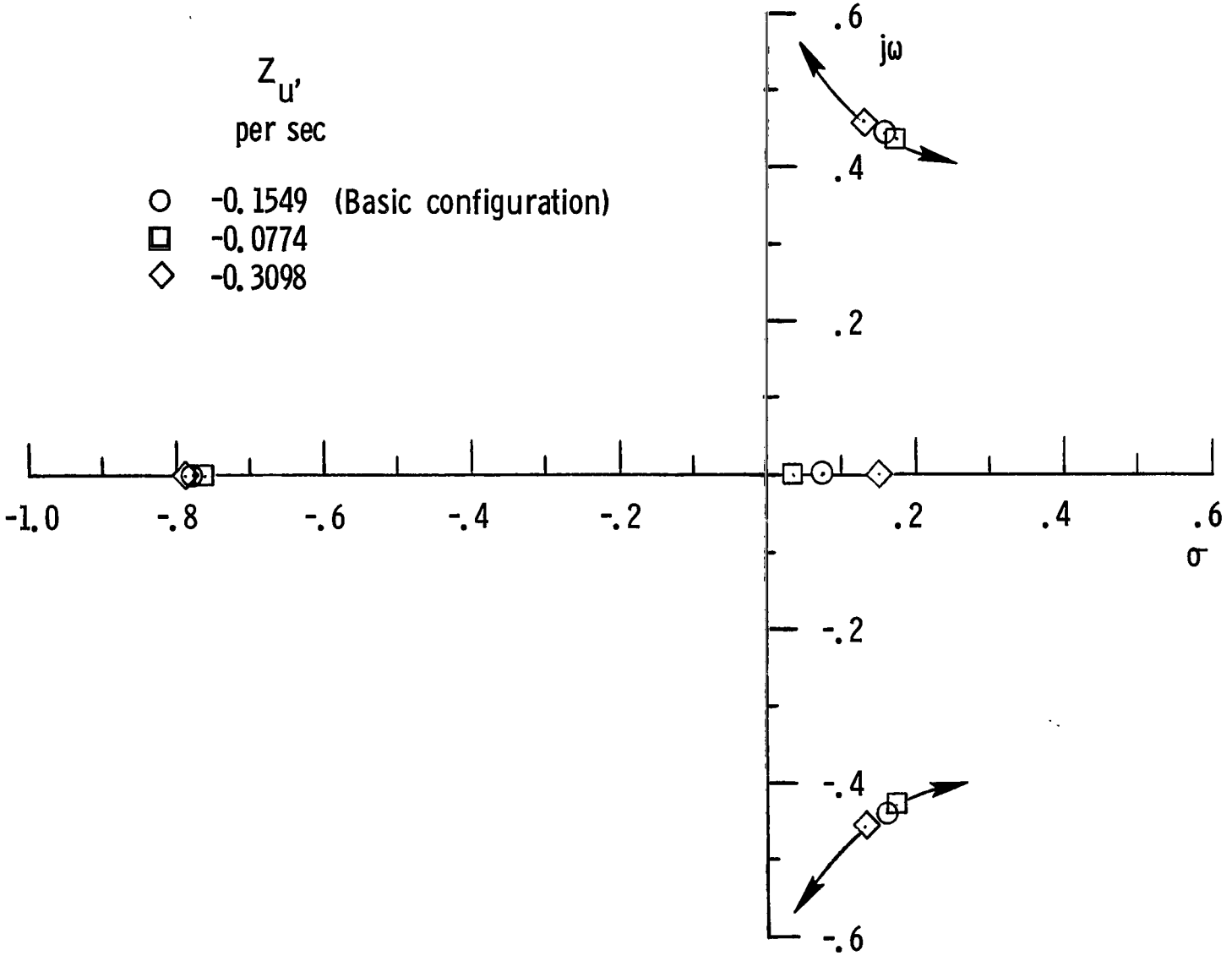

Figure 18.- Root locus for Z_u. $i_w = 65^0$.

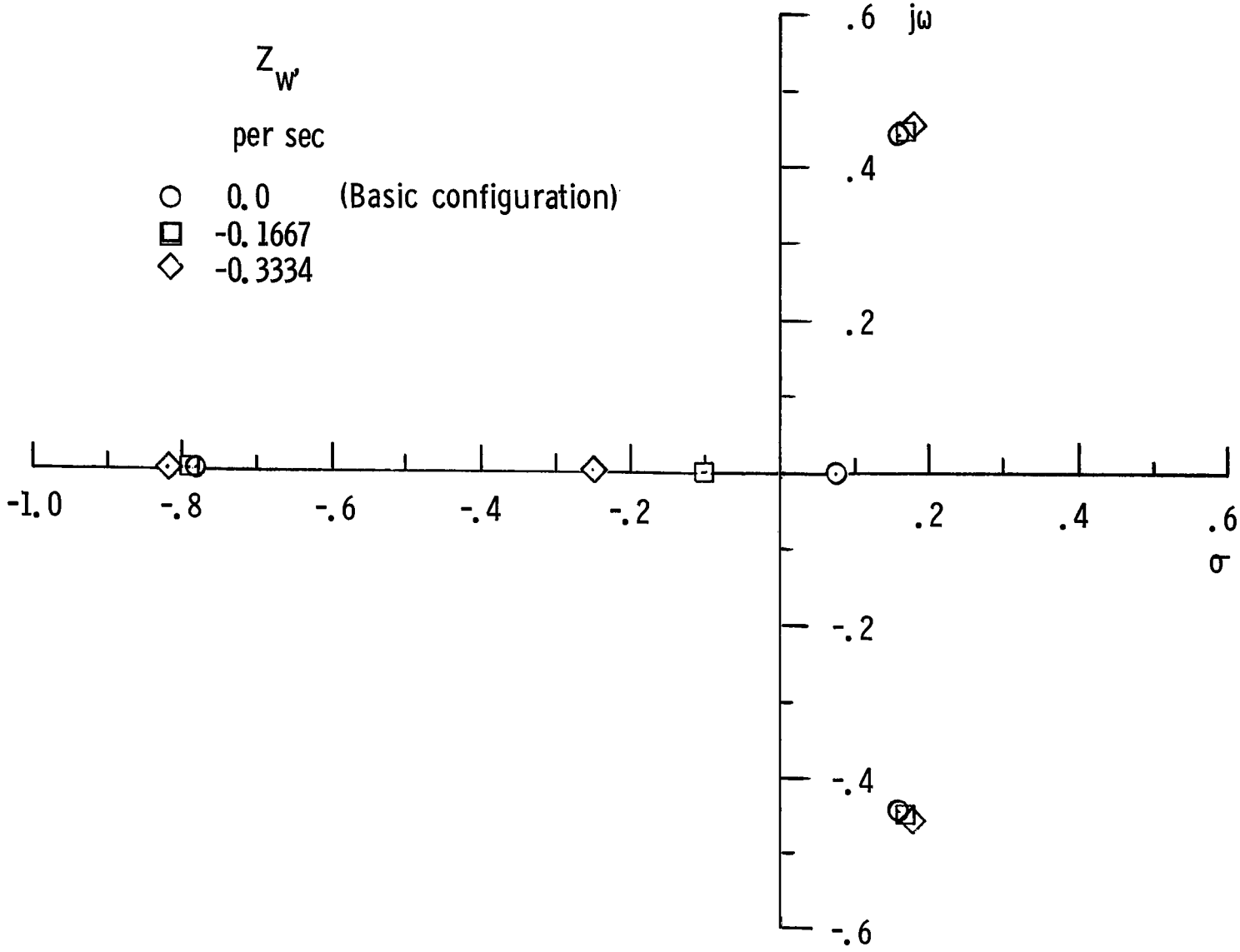

Figure 19.- Root locus for $Z_{w'}$. $i_w = 65^o$.

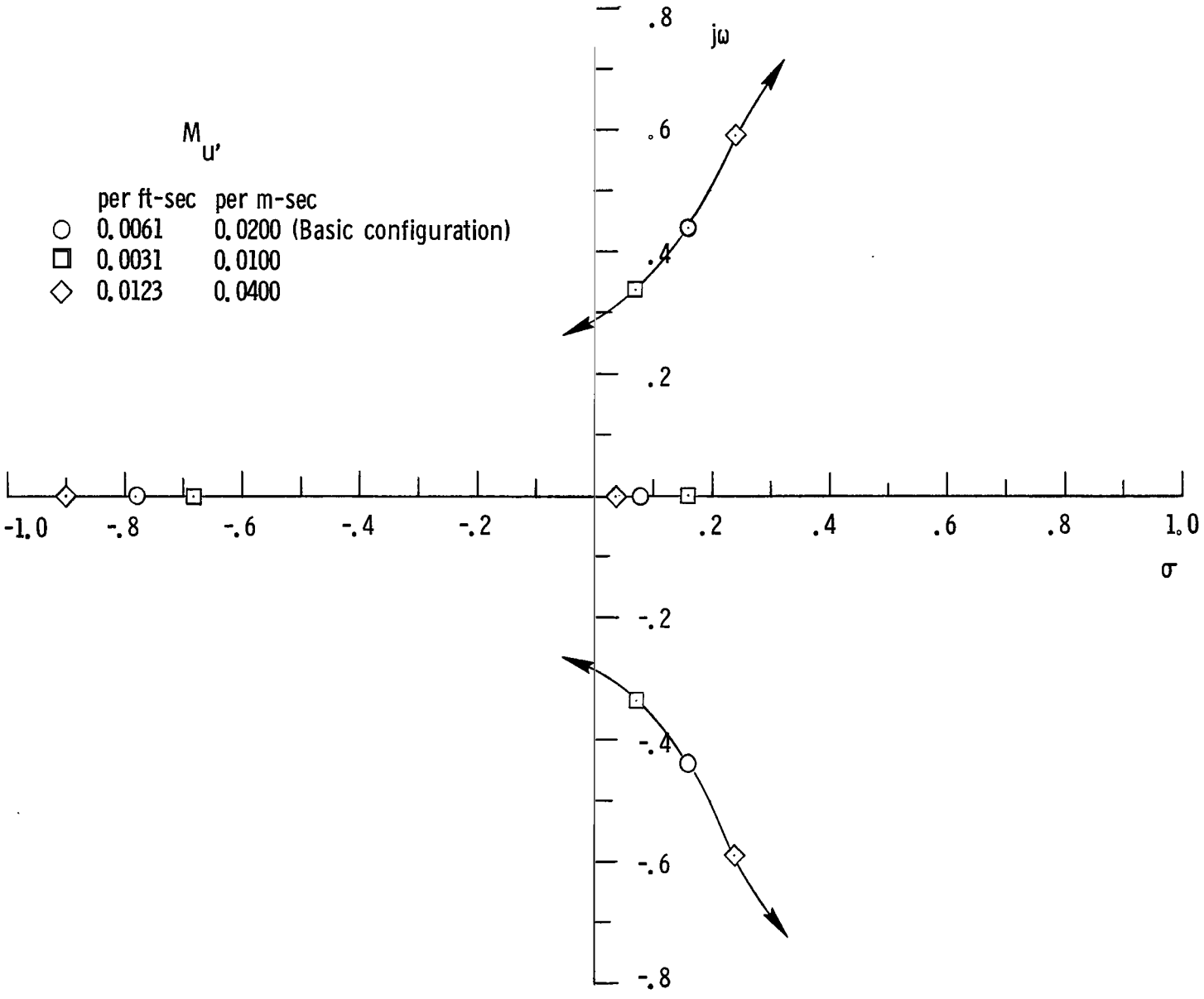

Figure 20.- Root locus for M_u. $i_w = 65^0$.

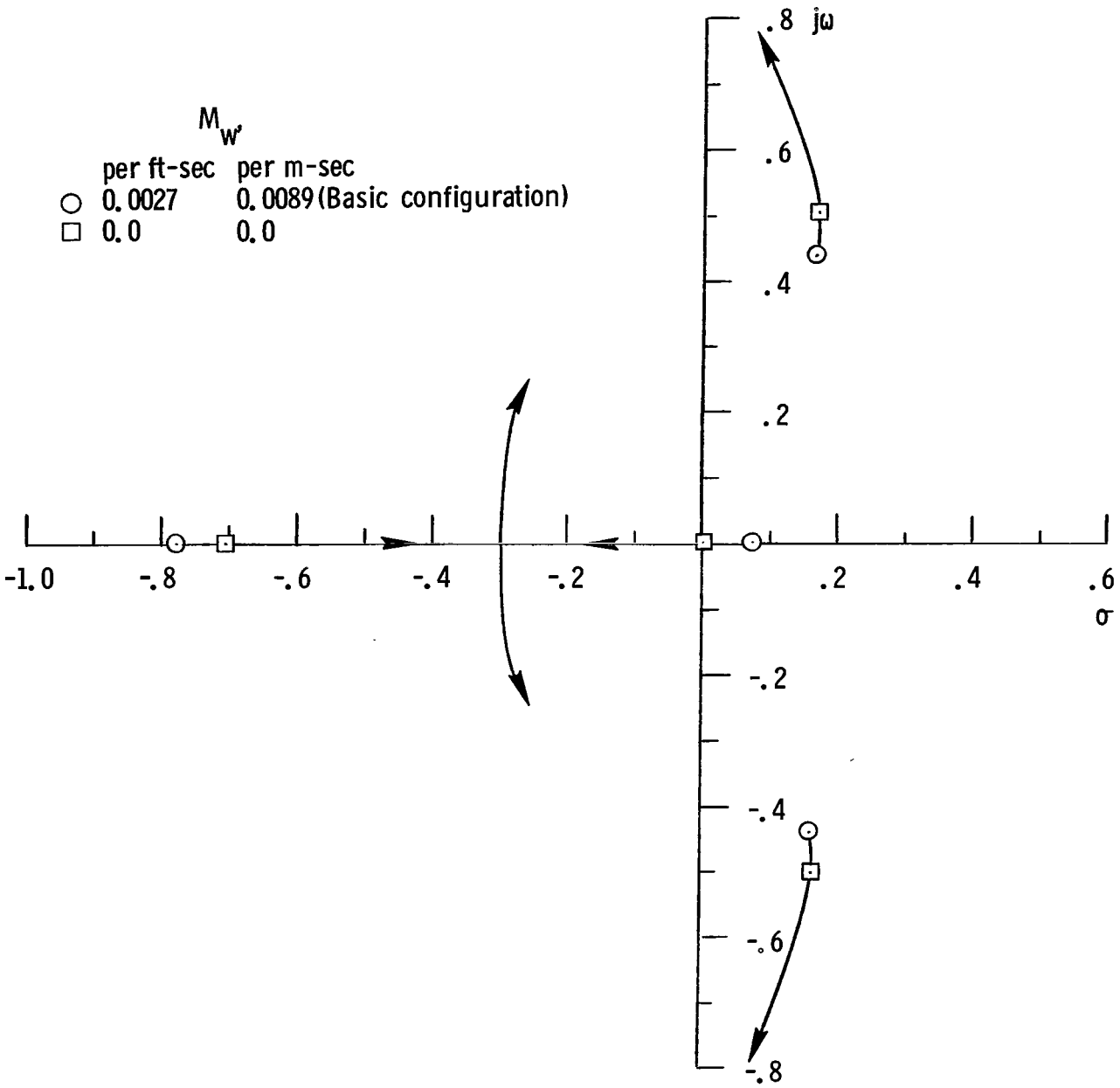

Figure 21.- Root locus for M_w. $i_w = 65^0$.

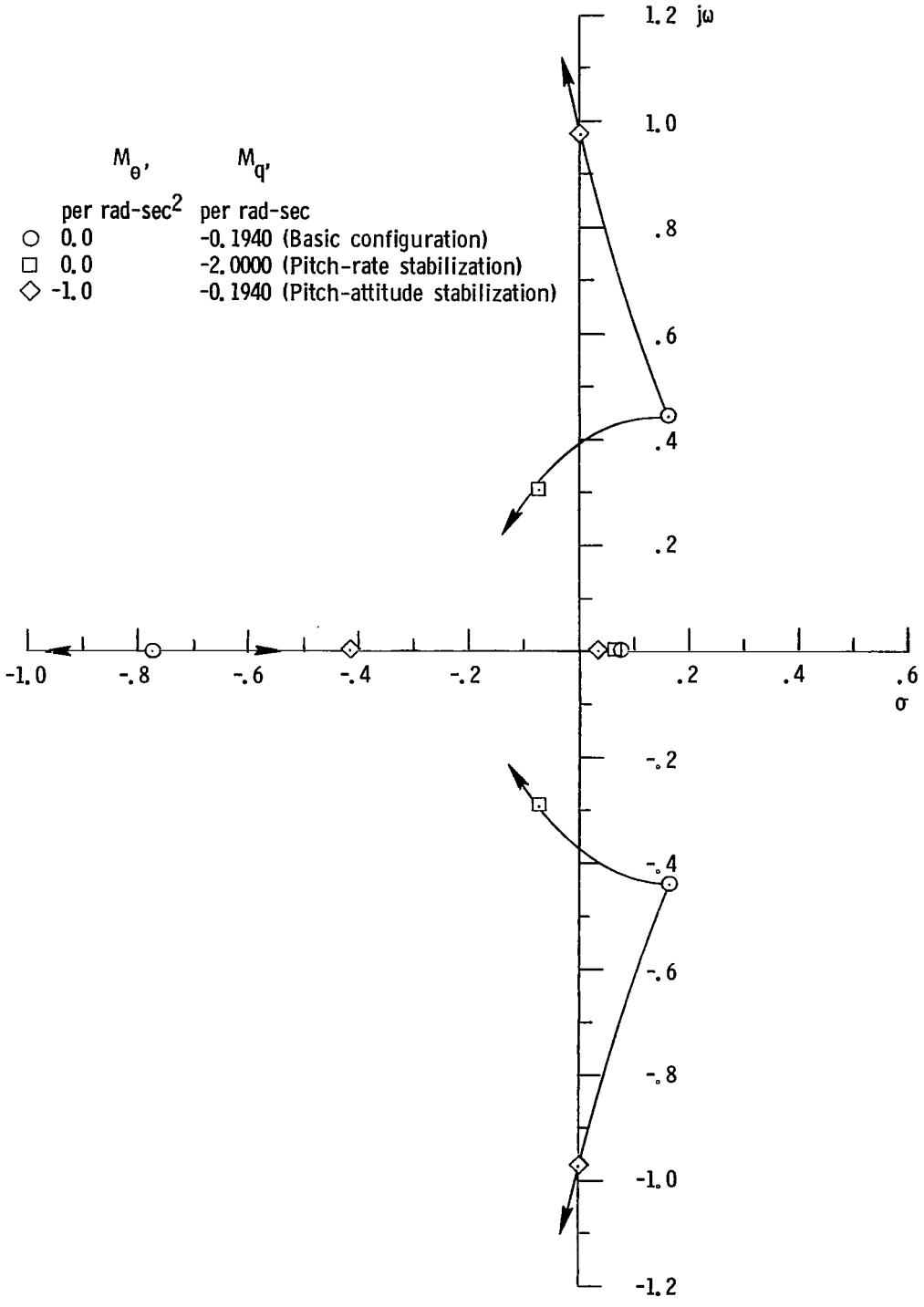

Figure 22.- Root locus for M_θ and M_q. $i_w = 65^0$.

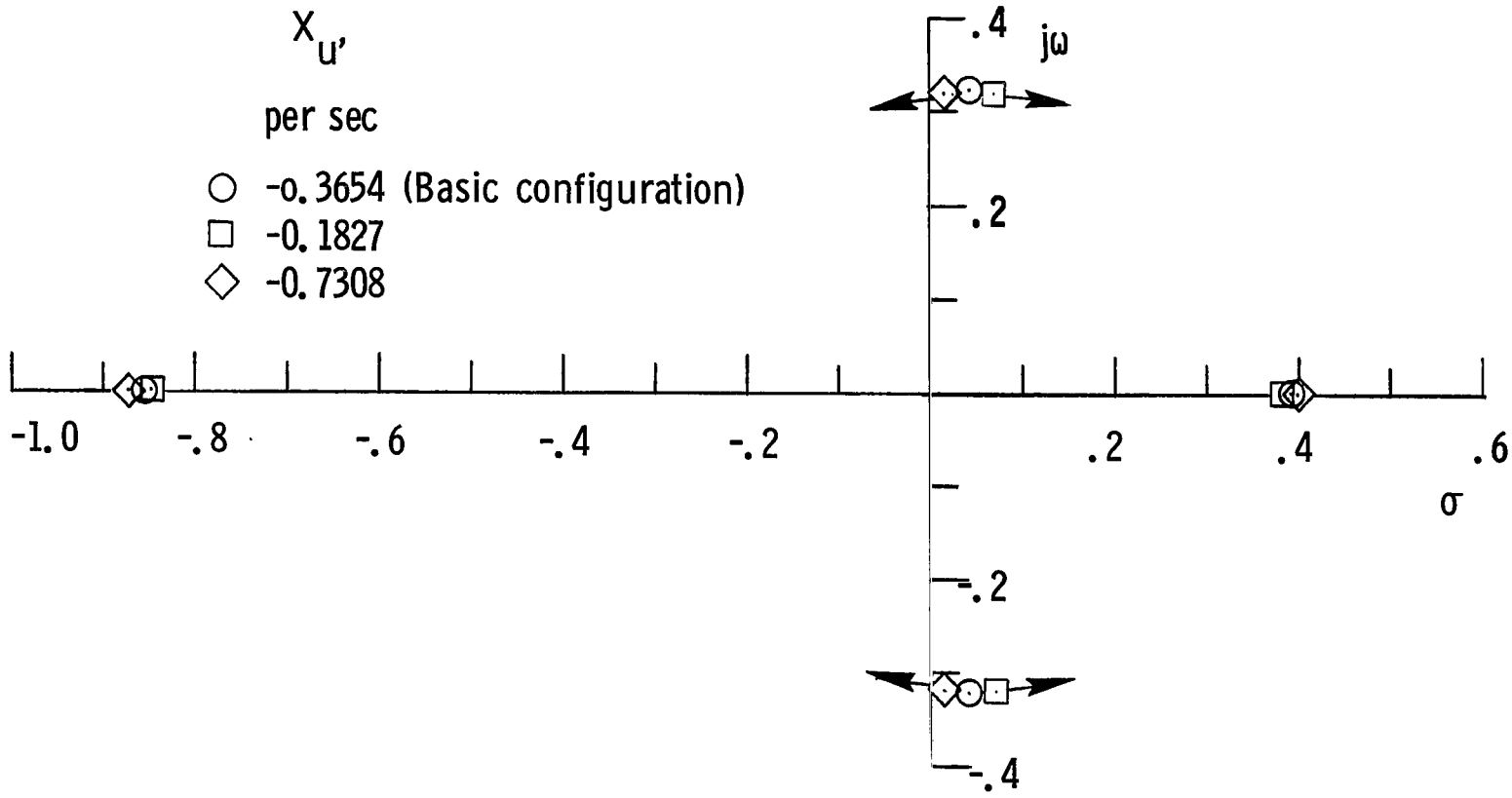

Figure 23.- Root locus for X_u. $i_w = 50^0$.

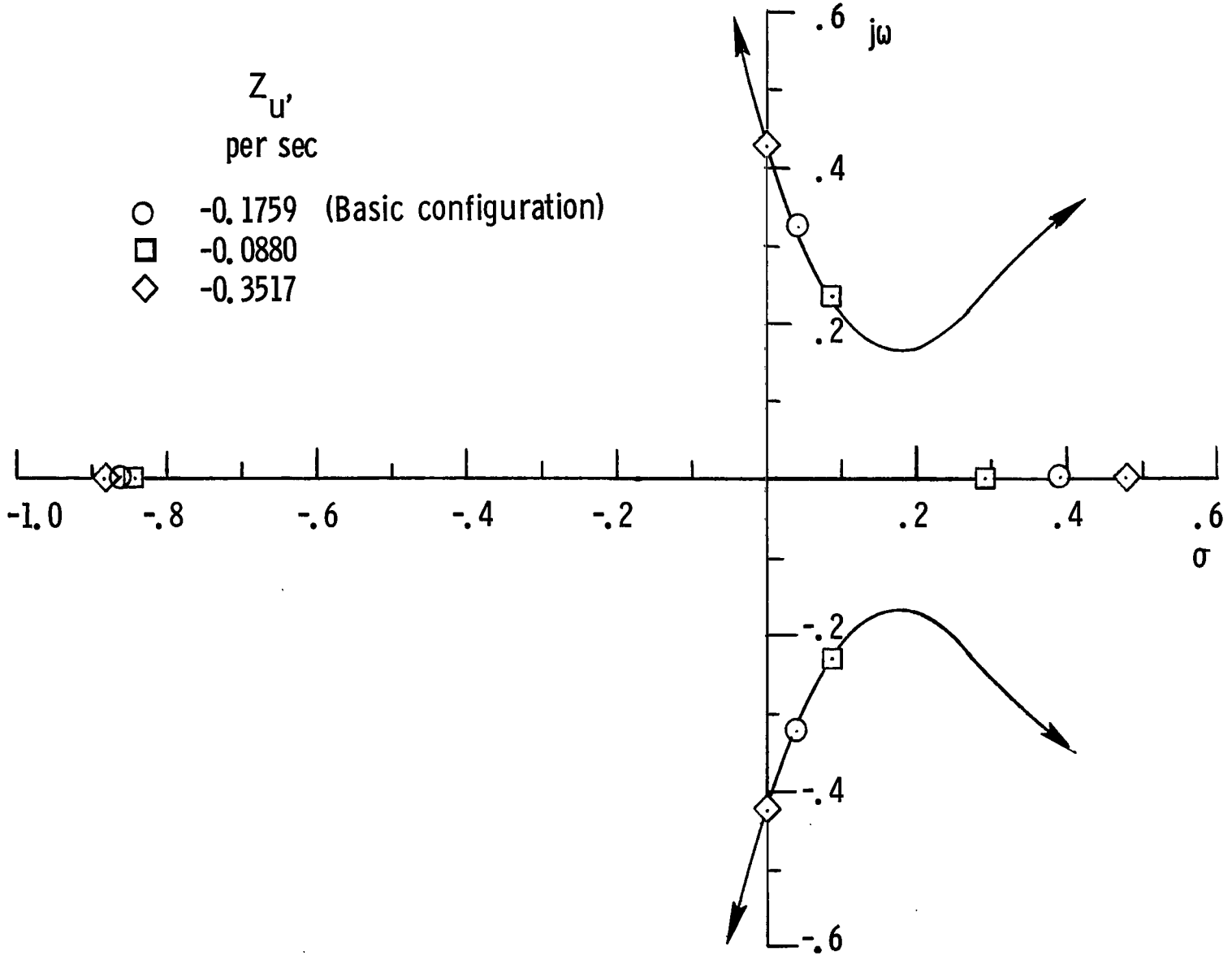

Figure 24.- Root locus for Z_u. $i_w = 50^0$.

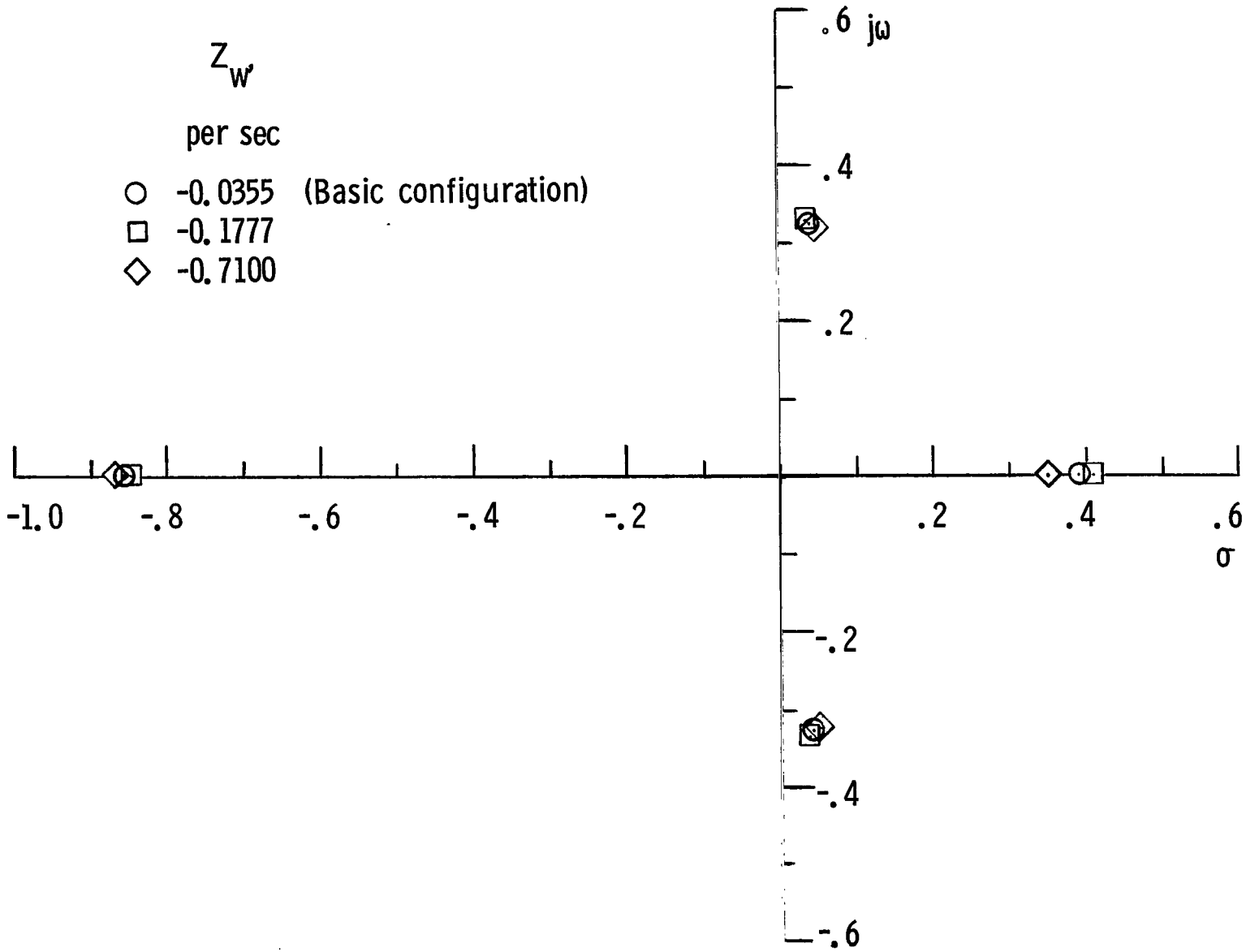

Figure 25.- Root locus for Z_w. $i_w = 50^o$.

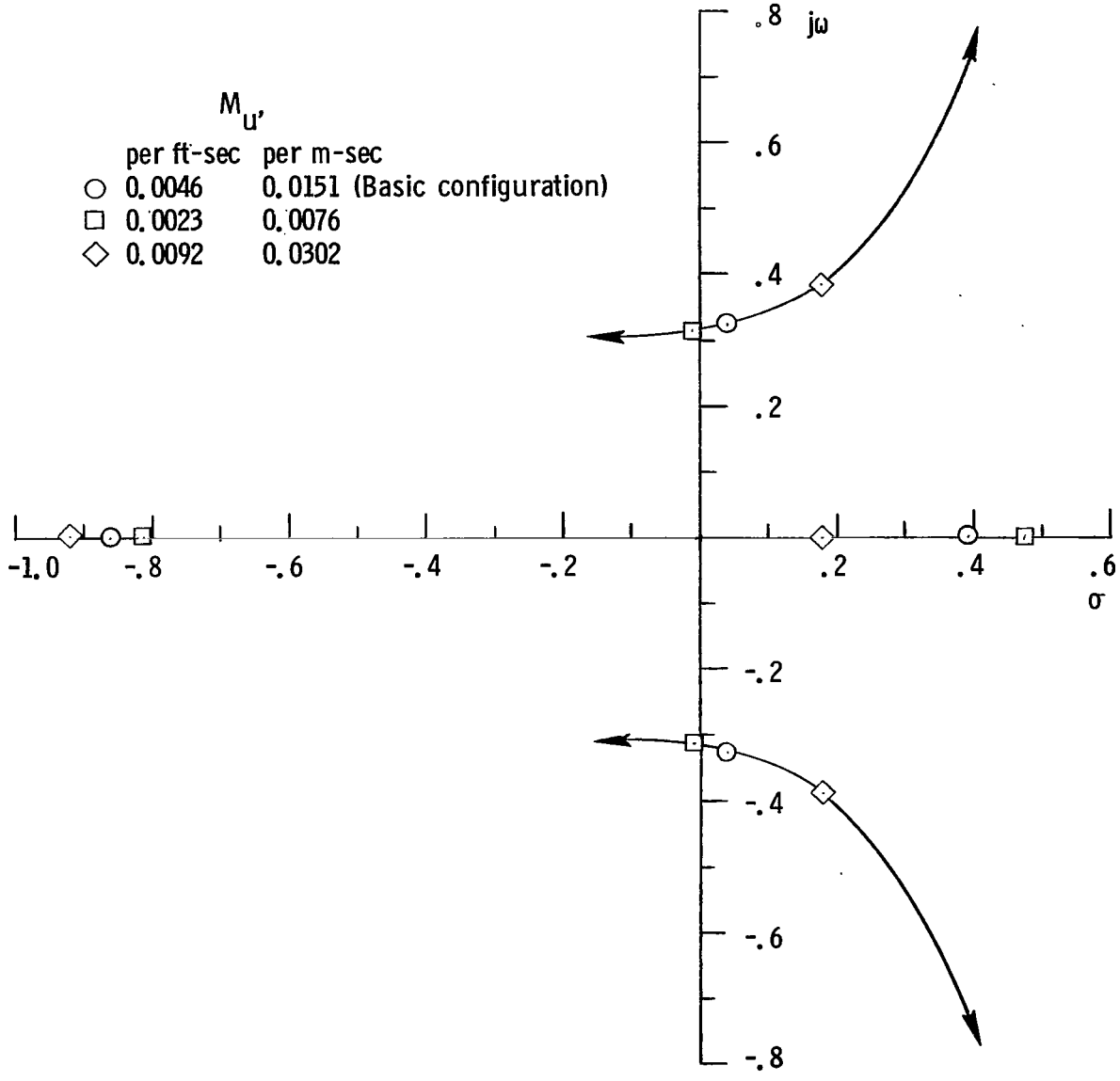

Figure 26.- Root locus for M_u. $i_w = 50^0$.

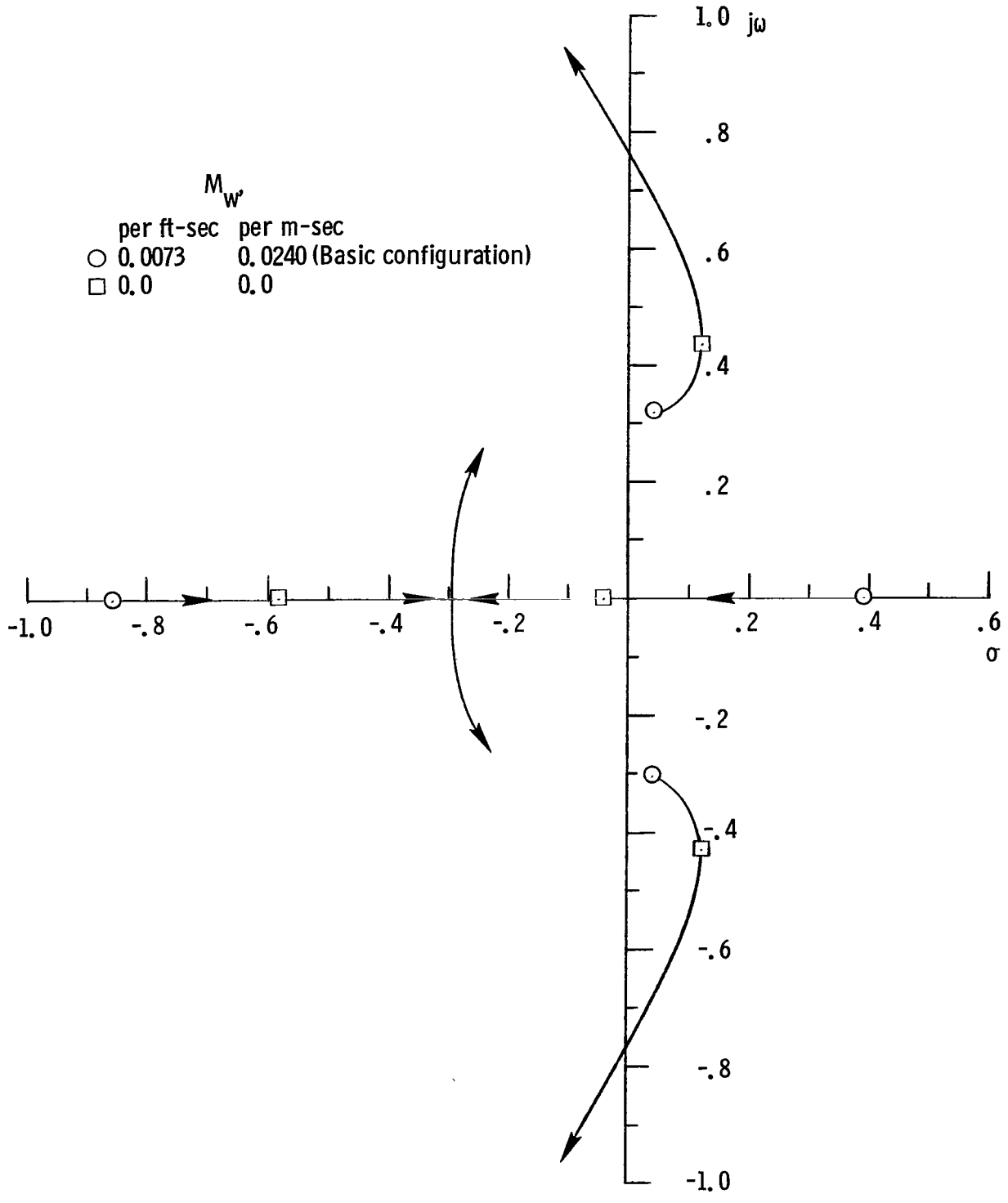

Figure 27.- Root locus for $M_{w'}$. $i_w = 50^o$.

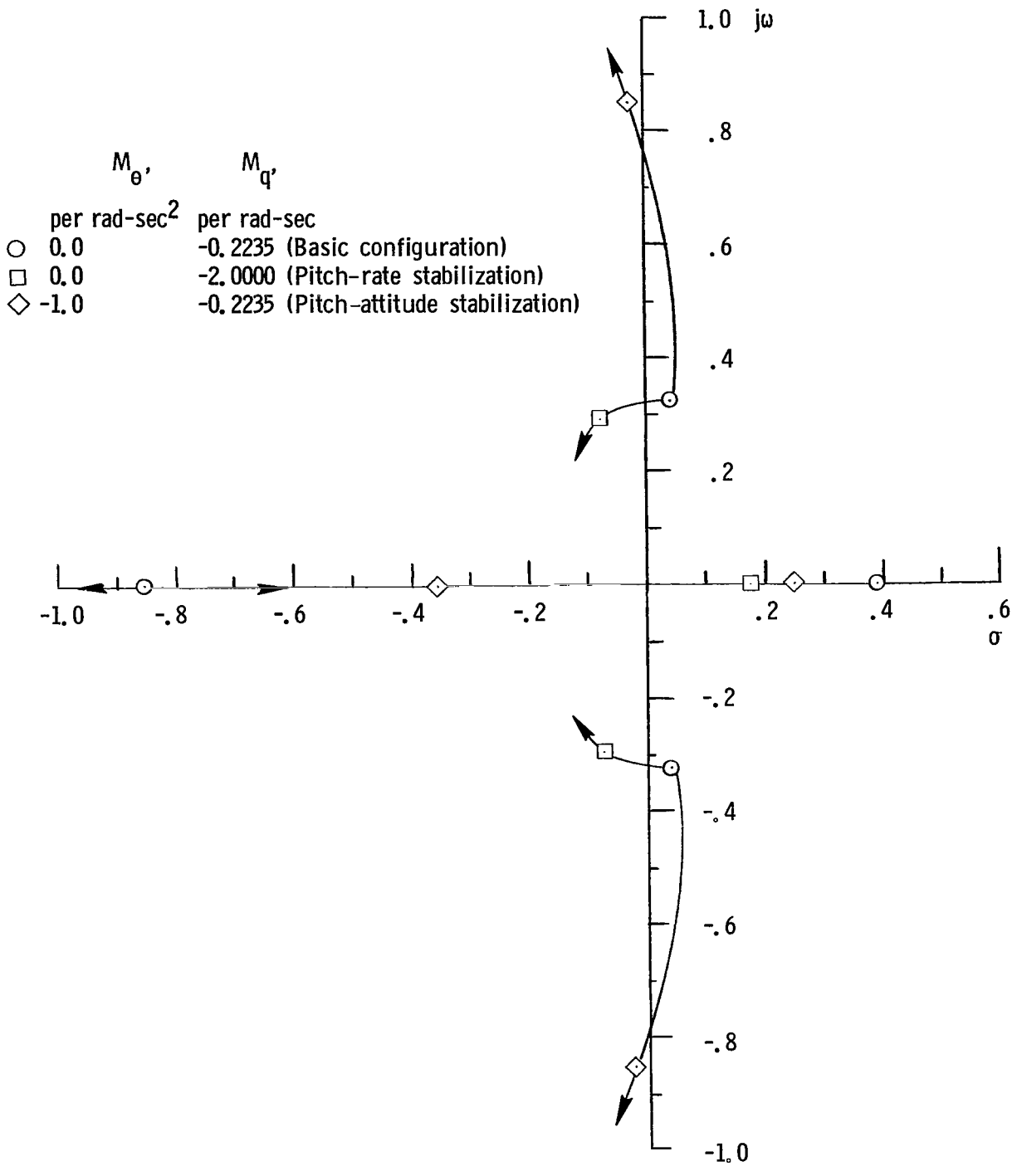

Figure 28.- Root locus for M_θ and M_q. $i_w = 50^0$.

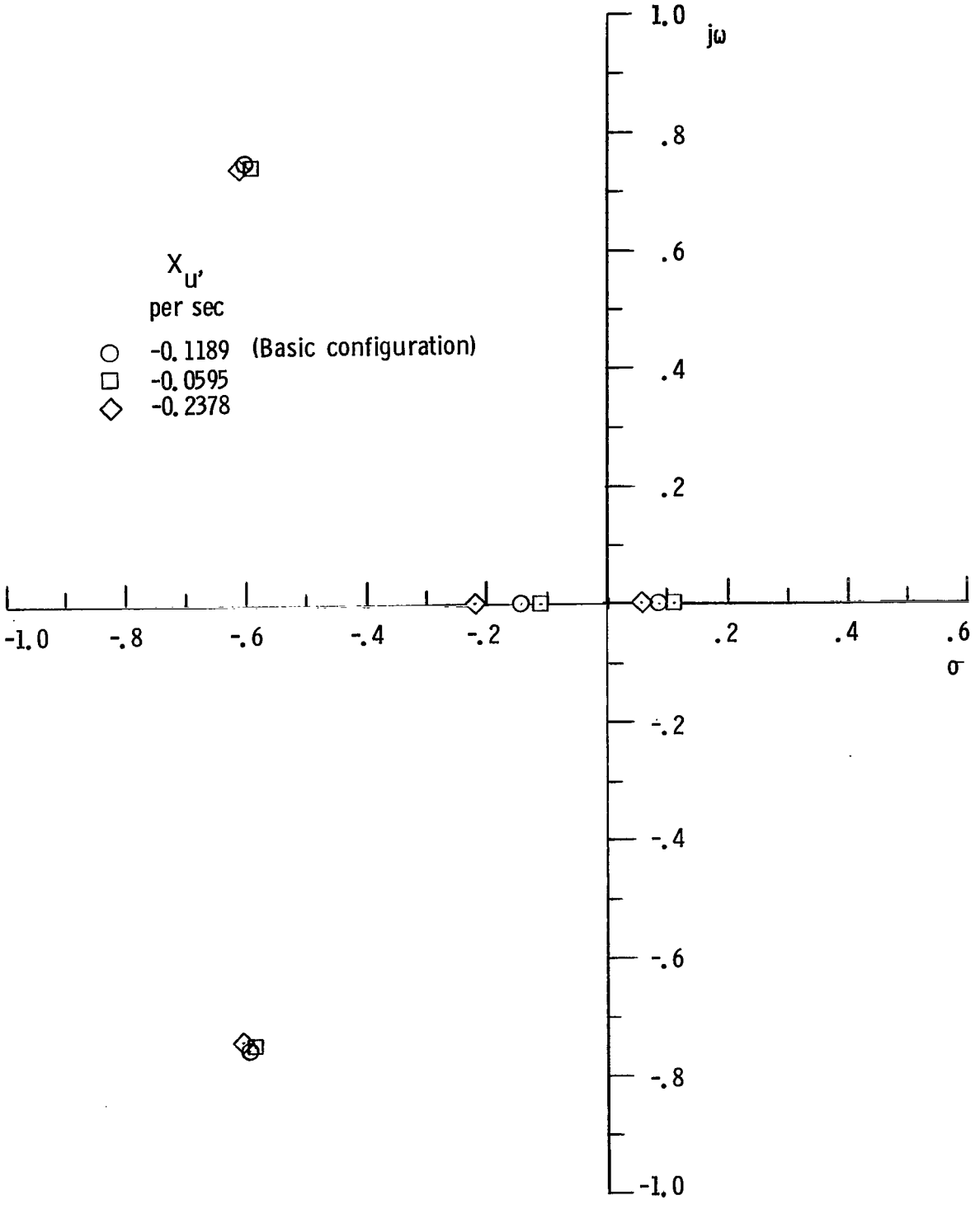

Figure 29.- Root locus for X_u. $i_w = 10^0$.

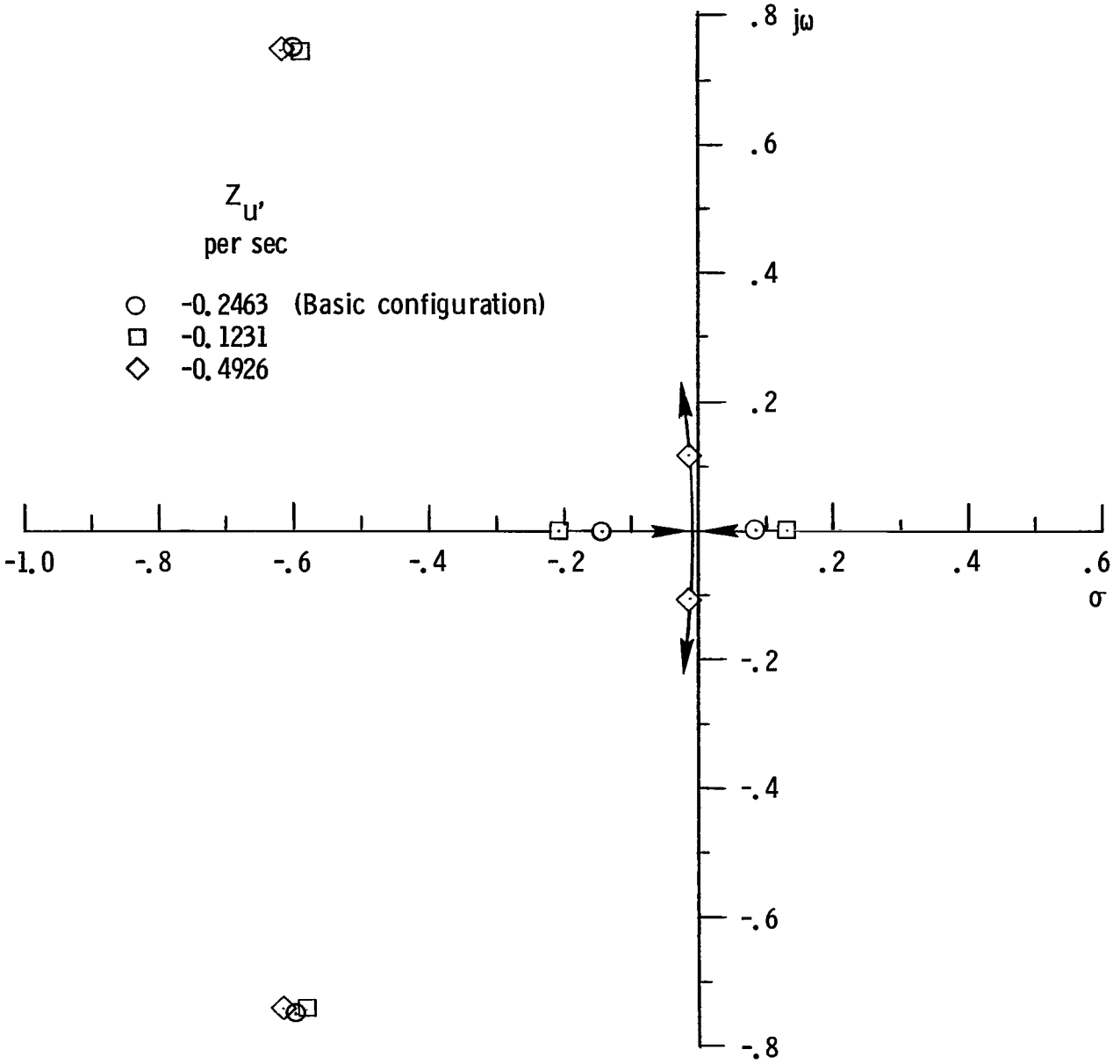

Figure 30.- Root locus for Z_u. $i_w = 10^o$.

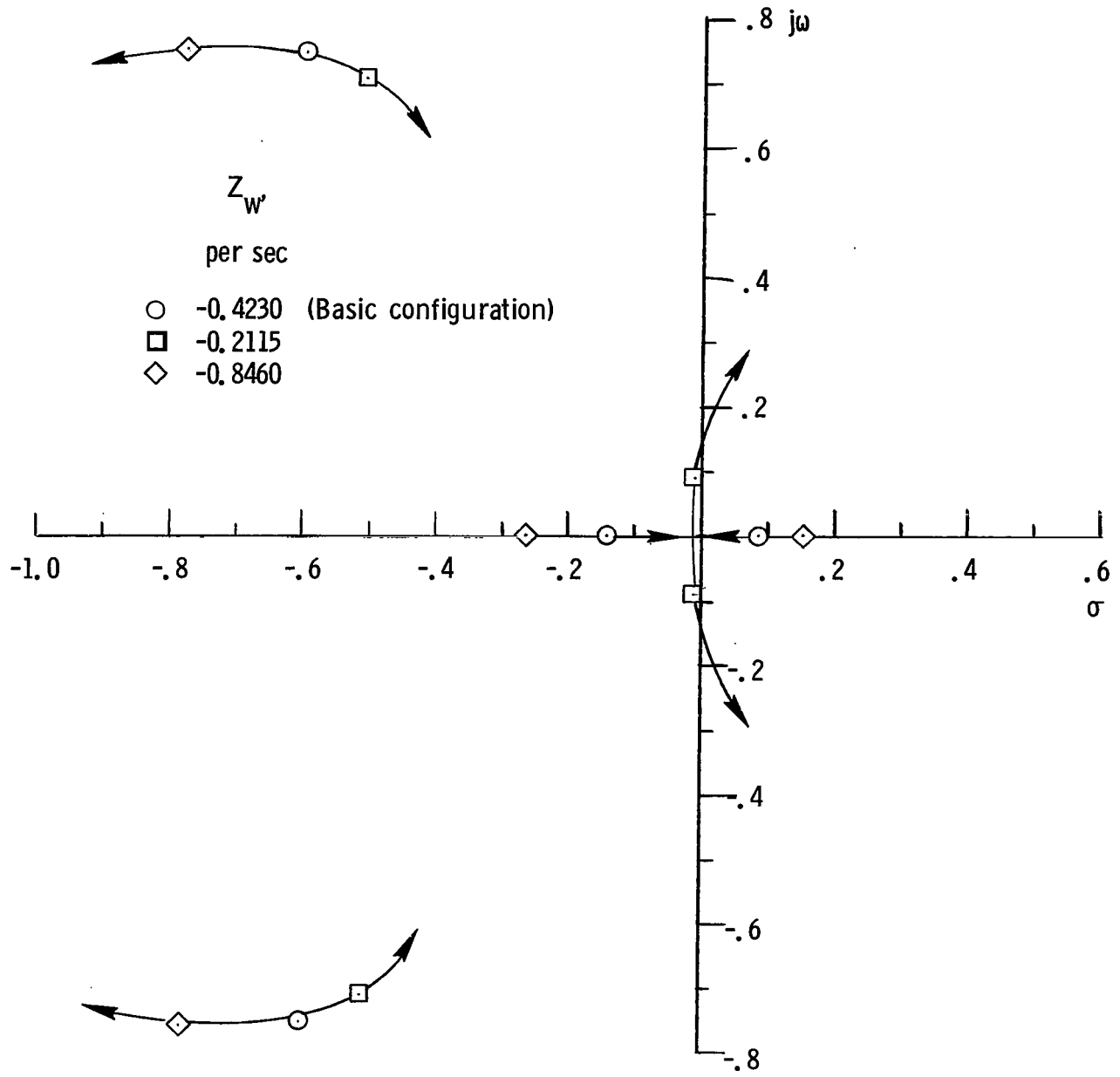

Figure 31.- Root locus for Z_w. $i_w = 10^0$.

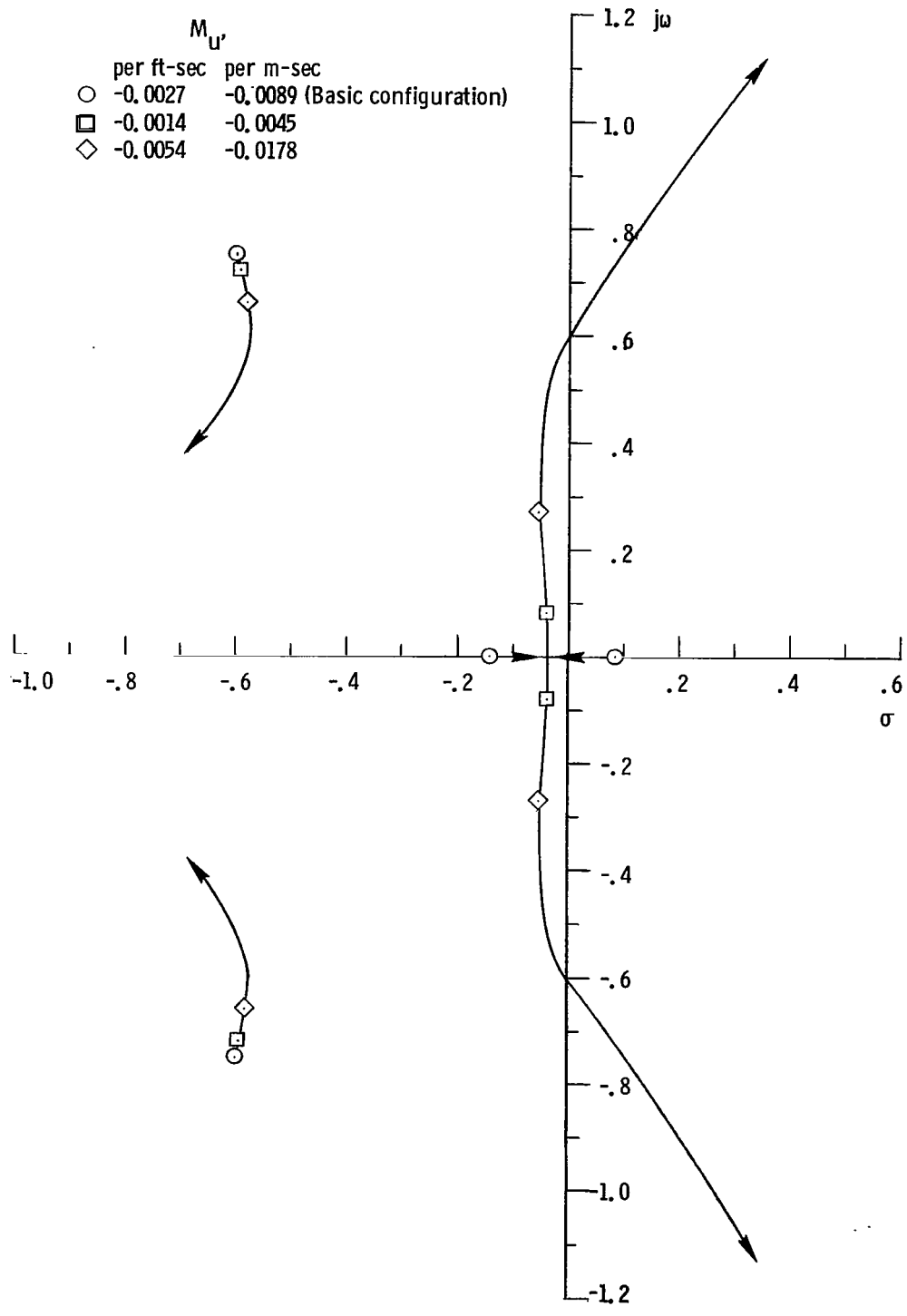

Figure 32.- Root locus for $M_{u'}$. $i_w = 10^0$.

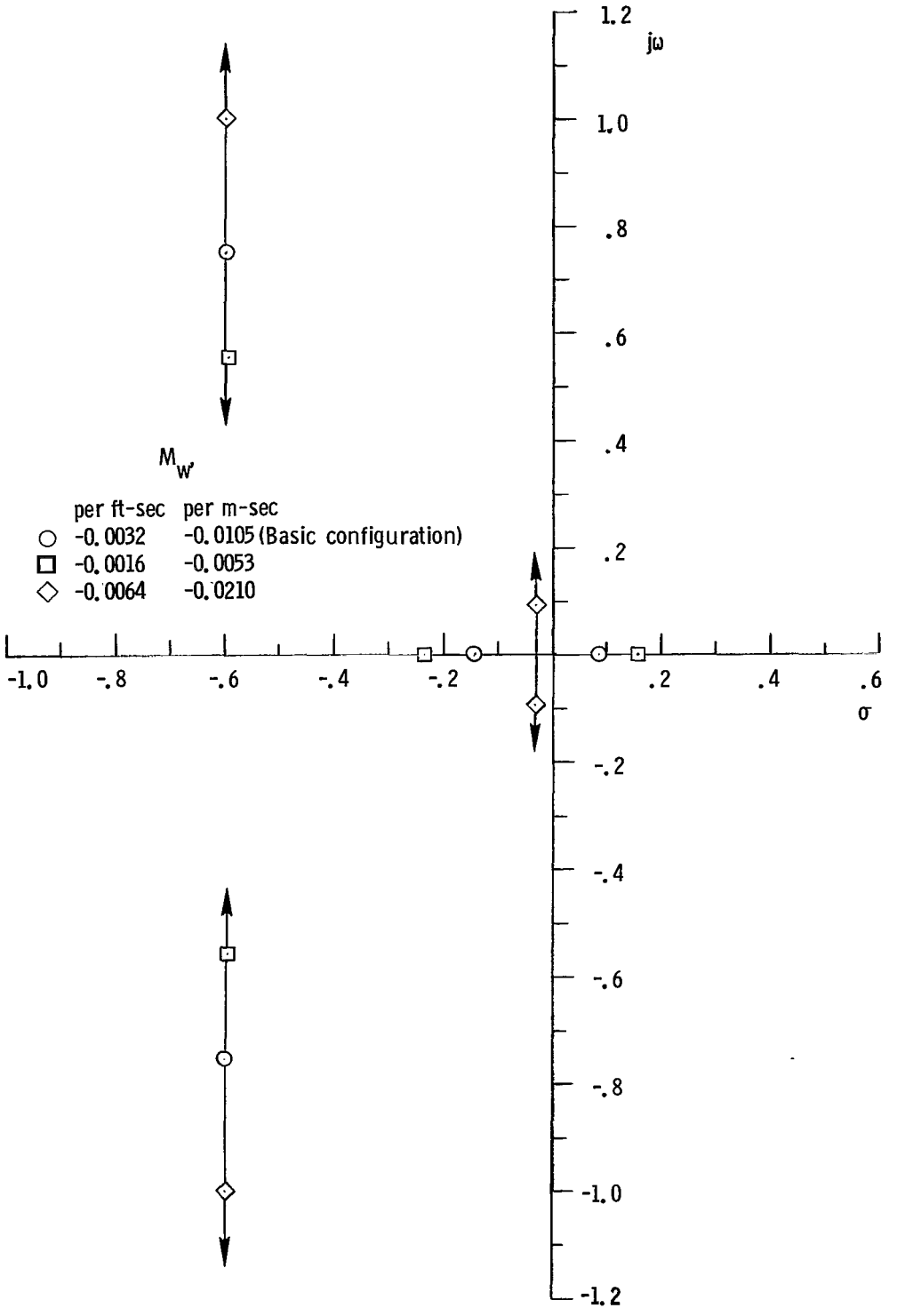

Figure 33.- Root locus for M_w. $i_w = 10^o$.

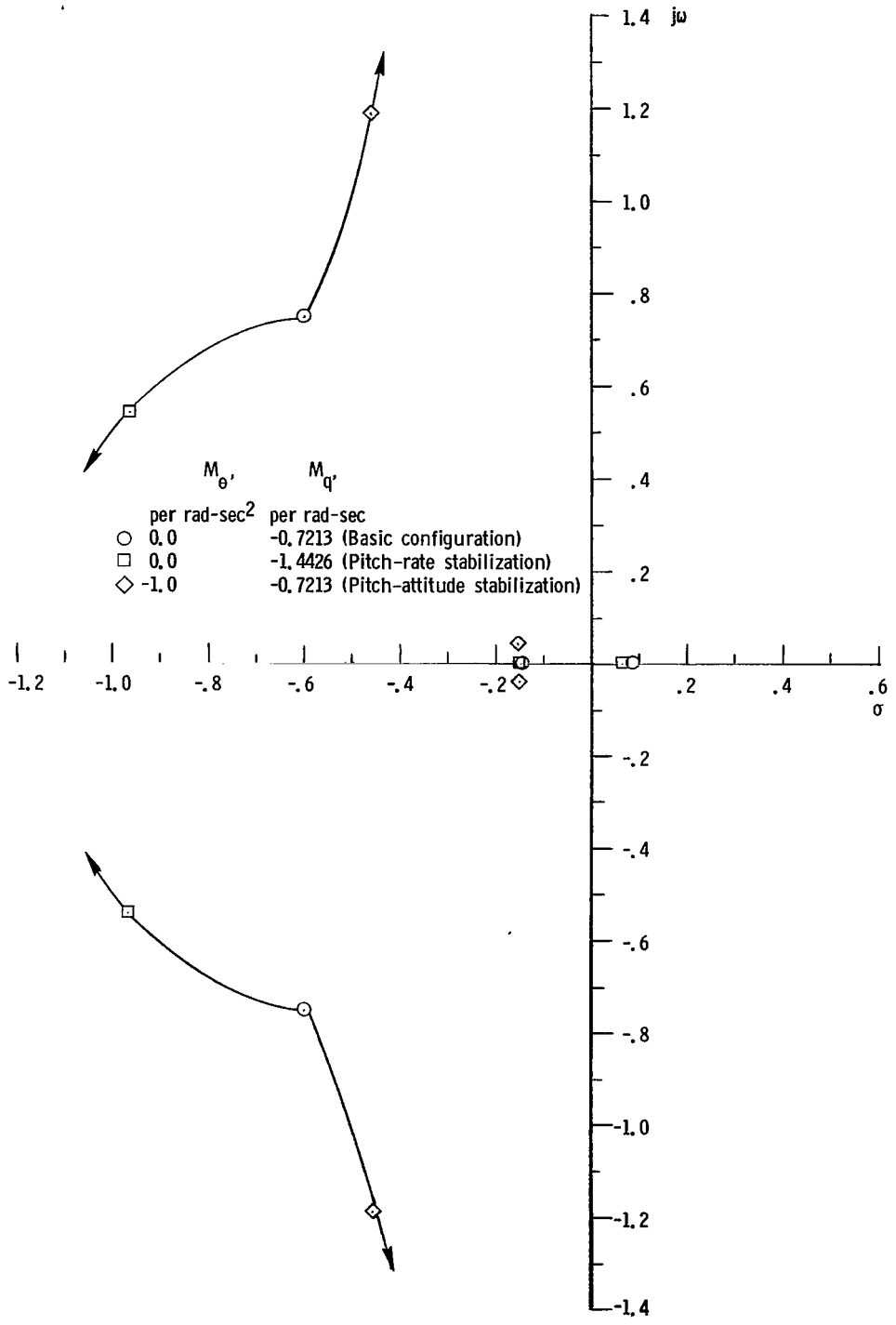

Figure 34.- Root locus for M_θ and M_q. $i_w = 10^0$.

National Aeronautics and Space Administration
WASHINGTON, D. C.

OFFICIAL BUSINESS

FIRST CLASS MAIL

POSTAGE AND FEES PAID
NATIONAL AERONAUTICS AN
SPACE ADMINISTRATION

POSTMASTER: If Undeliverable (Section 15
Postal Manual) Do Not Retur

"The aeronautical and space activities of the United States shall be conducted so as to contribute . . . to the expansion of human knowledge of phenomena in the atmosphere and space. The Administration shall provide for the widest practicable and appropriate dissemination of information concerning its activities and the results thereof."

—NATIONAL AERONAUTICS AND SPACE ACT OF 1958

NASA SCIENTIFIC AND TECHNICAL PUBLICATIONS

TECHNICAL REPORTS: Scientific and technical information considered important, complete, and a lasting contribution to existing knowledge.

TECHNICAL NOTES: Information less broad in scope but nevertheless of importance as a contribution to existing knowledge.

TECHNICAL MEMORANDUMS: Information receiving limited distribution because of preliminary data, security classification, or other reasons.

CONTRACTOR REPORTS: Scientific and technical information generated under a NASA contract or grant and considered an important contribution to existing knowledge.

TECHNICAL TRANSLATIONS: Information published in a foreign language considered to merit NASA distribution in English.

SPECIAL PUBLICATIONS: Information derived from or of value to NASA activities. Publications include conference proceedings, monographs, data compilations, handbooks, sourcebooks, and special bibliographies.

TECHNOLOGY UTILIZATION PUBLICATIONS: Information on technology used by NASA that may be of particular interest in commercial and other non-aerospace applications. Publications include Tech Briefs, Technology Utilization Reports and Notes, and Technology Surveys.

Details on the availability of these publications may be obtained from:

SCIENTIFIC AND TECHNICAL INFORMATION DIVISION

NATIONAL AERONAUTICS AND SPACE ADMINISTRATION

Washington, D.C. 20546